Satellite based analysis of environmental changes in the Monduli and Longido districts, Tanzania




S.L. Verhoeve

Utrecht University

Satellite based analysis of environmental changes in the Monduli and Longido districts, Tanzania

MSc Thesis

August 2019

Author: Steye Laurens Verhoeve
Student number: 4119274
E-mail: steyeverhoeve@gmail.com
First supervisor: Dr. Ir. Geert Sterk
Second supervisor: Dr. Maarten Zeylmans van Emmichoven

MSc programme: Earth surface and Water
Faculty: Geosciences
Department: Physical Geography
Course: Graduation research, Earth Sciences (GEO4-1520)
Utrecht University

ECTS: 45

Abstract

Knowledge on seasonal land cover is important to pastoralists and farmers as it aids in understanding the patterns throughout the year. This study was carried out to (a) understand the long-term land-use and land-cover (LULC) change; (b) the vegetation dynamics and ecosystem resilience; and (c) gain insight in the local perspective on these factors. The study was carried out in the Monduli and Longido districts in northern Tanzania. Multi-temporal satellite imagery from the Landsat missions from 1985 to 2019 were used. Using a RandomForest classifier 32 images were classified based on a training dataset for the wet or dry season. The extend of the LULC classes was determined. This resulted in a highly variable class sizes. This was in disagreement of the classified maps with field observations and visual interpretation of satellite imagery. Questions were raised on comparable results from other studies. From eight different vegetative areas the NDVI was computed over time. Of the rural areas, only forested area showed a significant increasing trend, the other regions had no trend. The agricultural areas all showed an increase in the annual averaged NDVI. The intra-annual NDVI is strongly correlated to the seasonal precipitation. For all areas during a dry year the trend was typically lower and during a wet year typically higher than normal NDVI values. The NDVI values consecutively to a dry year were lower than normal for the natural systems but did not show any deviation from normal in the second consecutive year. This indicates the strong resilience of the systems to short-term droughts. The inhabitants noted an increase in temperature, trees, competition for grazing and unreliable rains. This has an effect on the availability of good quality grass. The change in temperature has been measured by meteostations. The change in vegetation was not detected by any change in NDVI.

Key words*: LULC change, Google Earth Engine (GEE), Landsat, vegetation dynamics, NDVI, semi-arid*

Contents

1 Introduction

Land degradation is one of the world's major socio-economic and environmental problems, affecting over a billion people in 110 countries worldwide (Middleton and Thomas, 1997). According to the World Atlas on Desertification, "*land degradation leads to a long-term failure to balance demand for and supply of ecosystem goods and services*" (Cherlet et al., 2018). These ecosystem goods and services is what all life on our planet is entirely dependent on (Pullanikkatil et al., 2016). The provided goods and services consist out of a wide range, such as food, clean water, disease management and climate regulation (Millenium Ecosystem Assessment, 2005).

Grassland ecosystems are under tremendous pressure from a rising demand for natural resources and animal products to cope with a sharply increasing human population. Agricultural expansion accompanied by high water consumption and the conversion of natural landscapes into cultivated lands have led to severe land degradation all over the world (Tangud et al., 2018; Pullanikkatil et al., 2016; Wickama et al., 2014). Land degradation undermines the land's productivity and contributes to the degradation of ecosystem services. The degradation is being borne disproportionately by the poor and is sometimes the decisive component which results in poverty and social conflict (Millenium Ecosystem Assessment, 2005; Interim Secretariat, 1994). The loss of productive land is part of a vicious circle for many rural people in the developing world in which land degradation can be both the cause and the consequence of poverty (Tal and Cohen, 2007).

East Africa is home to thousands of pastoralists who herd their livestock in the semi-arid to arid areas of the region. The pastoralist have been challenged by means of restrictions on mobility, privatization of land, and substitution of pastoralism with less sustainable forms of livestock keeping. According to the WISP (2008) mobility and locally owned institutions for land management would positively influence biodiversity conservation and sustainable land management. One of the pastoralist groups, The Maasai, a Nilotic ethnic group of semi-nomadic pastoralists and agro-pastoralists, live on the rangelands of southern Kenya and northern Tanzania. Their rangelands cover 150,000 km^2 and are known for the iconic pastoralist population ($\sim$1,297,000 inhabitants) and its high mammal concentrations ($\sim$2 million) (Homewood et al., 2009). Currently the area is undergoing rapid changes, perceived to be both positive and negative. The alleviation of poverty is an important positive change, but the wildlife populations are dwindling and the environmental sustainability is decreasing due to changes in land-use and land-cover (LULC) (Homewood et al., 2009).

In order to foster both developments in a positive way, it is important to understand the changing LULC and the people livelihoods. The LULC in this area is largely dependent on the amount of rainfall. Intensive rainfall and extensive droughts alternate in the region (NBS, 2017; Galvin et al., 2004) which affects the forage availability, livestock production and also the livelihoods of the people. Long term LULC change in Tanzania has been studied with the use of remote sensing data (1980s – 2015)(Bergh, 2016; Kiunsi and Meadows, 2006; Mtui et al., 2017). These studies have shown that the natural and semi-natural vegetation has decreased by both anthropological factors and ecosystem dynamics. From the studies it was concluded that urban area, agricultural area and bare soil has increased significantly, while the extensiveness of natual lands such as savannah has decreased. However, these studies do not agree on the amount of LULC change for the different LULC classes. Due to the use of limited datasets the studies could be biased e.g. by climatic factors and classification errors(Conroy, 2001; Degen, 2015; Iqbal and Khan, 2014; Maerker et al., 2015; Quénéhervé et al., 2015).

Knowledge on seasonal land cover is important to pastoralists and farmers as it aids in understanding the patterns throughout the year and aids in identification of times and

location with optimum vegetation growth. Understanding the change of LULC can allow quantifying and monitoring trends in agricultural activities, forest cover, disease transmission and land degradation (Midekisa et al., 2017). A change in the LULC has affected the wildlife species in and around national parks and game-controlled areas (protected areas, PAs) all over Tanzania. Wildlife encounters are more frequent with humans, settlements and agricultural activities due to the establishment and expansion of villages, population growth, and a change in agricultural policies that were established in 1974 and 1983 to improve social welfare of the inhabitants (Prins, 1987). These policies have caused enhanced land degradation because of the increased amount of settlements, livestock herds, farming and mining activities (Msoffe et al., 2011; Mwalyosi, 1992; Prins, 1987). An area commonly cited as having serious land-degradation problems in terms of overgrazing and soil erosion is the Monduli and Longido districts in northern Tanzania (Blake et al., 2018; Kiunsi and Meadows, 2006). This is an area typical of the drylands of the Rift Valley.

In this context, this study will focus on the land-use and land-cover changes in northern Tanzania from 1985 to 2019, and the subsequent consequences regarding livelihood strategies. The threefold objective of this study is:

- to assess long term land-use and land-cover changes using multitemporal and multispectral satellite imagery from the Landsat missions of the Monduli and Longido district, northern Tanzania;
- to assess seasonal land cover dynamics and ecosystem resilience to climatic factors;
- and to gain insight into the local perspective of the land-use and land-cover change and vegetation dynamics.

2 Materials and methods

2.1 Study area

Tanzania is divided into thirty-one regions, which are all divided into districts. The study area of this research are the administrative Monduli and Longido districts in the Arusha region, northern Tanzania (Figure 3)(UN OCHA ROSA, 2018). The districts are situated between latitudes 2.20°and 4.50°S and between longitudes 36.00°and 37.30°E. The total area covers approximately 16,000 km^2 and has 282,112 inhabitants (158,929 and 123,153, Monduli and Longido district respectively) (NBS, 2013). It is an important area for wildlife conservation, since large parts of the Arusha Region are PAs, including or bordering the Manyara, Arusha, Tarangire, Mount Kilimanjaro and Serengeti National Park, and the Ngorongoro Conservation Area.

For many years the Maasai people occupied this area. Most of the inhabitants are from the Maasai ethnic group (40%), 20% is Waarusha and the other 40% is not indigenous (Decentralized Climate Finance Project, 2019). The Maasai originally live in small villages or *boma* which consists of 20 up to 200 people living in huts made from timber and manure. The total population of Maasai has been reported as numbering 1,290,000, based on the number of people speaking Maa, a member of the Nilo-Saharan linguistic family. The Maasai used to live as pastoralists, herding livestock such as cows, goats and sheep for their livelihood (Homewood et al., 2009). Due to the strong seasonality of the precipitation and the flourishment of vegetation, it is important for the Maasai to be able to migrate to find other pastures and resources (Fratkin, 2001).

The study area is characterized by a semi-arid landscape. It is characterized by four climatic seasons (Figure 2). A short wet season is from November to December, followed by a short hot season (Jan-Mar) until the long rains start which occur typically from March to May. From May to October a long dry season can be identified with cooler temperatures. The mean annual rainfall is between 450 and 1,200 mm, averaging around 750 mm annually (Figure 4). The lower lying areas receive a mean annual rainfall of about 650 mm, whereas the highlands receive 1,000 mm to 1,200 mm per year on average (Quénéhervé et al., 2015; Prins, 1987). The average temperature is between 20-25 degrees Celsius (°C), with a minimum of 11 °C in July to September and a maximum high temperature of 31 °C in January and February (Conroy, 2001; TMA, 2019).

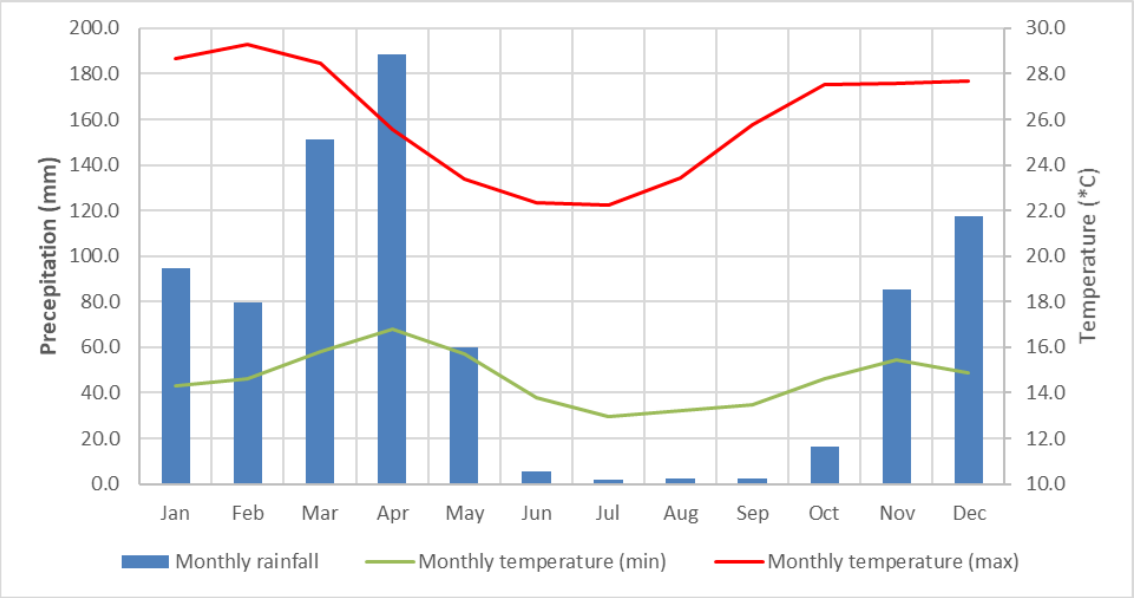

Figure 2: Annual precipitation and temperature variability. Source: TMA (2019)

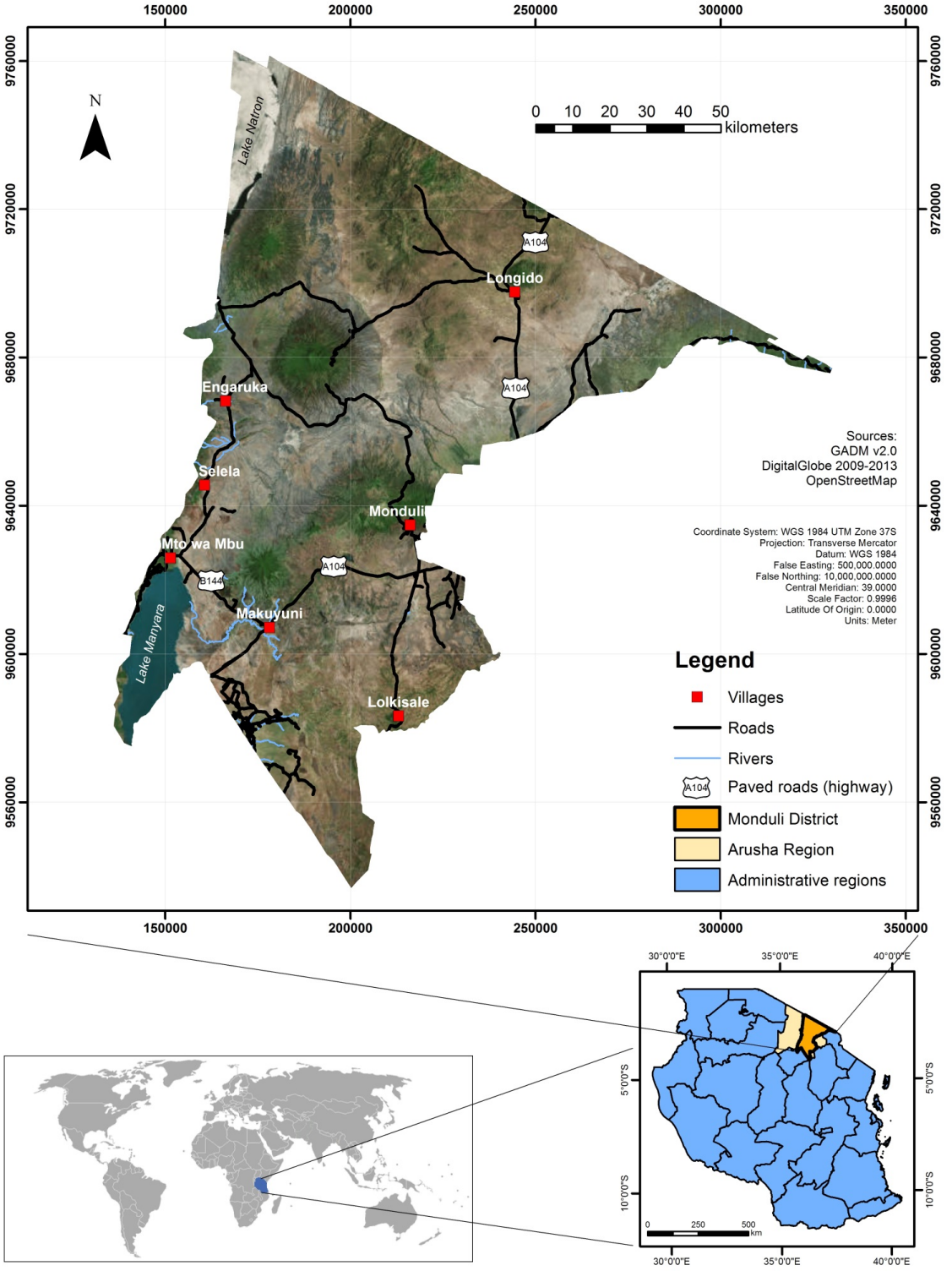

Figure 3: Study area: the Monduli and Longido districts, Tanzania. Source: Bergh (2016)

The physical characteristics of the area, such as morphology, geology and soils, are strongly influenced by tectonic activities and volcanism (Kiunsi and Meadows, 2006). The characteristics have influenced rainfall distribution, vegetation types and wildlife of the area. The Monduli district is part of the Lake Manyara catchment. Lake Manyara, part of an endorheic basin, is the southernmost lake within the eastern arm of the East

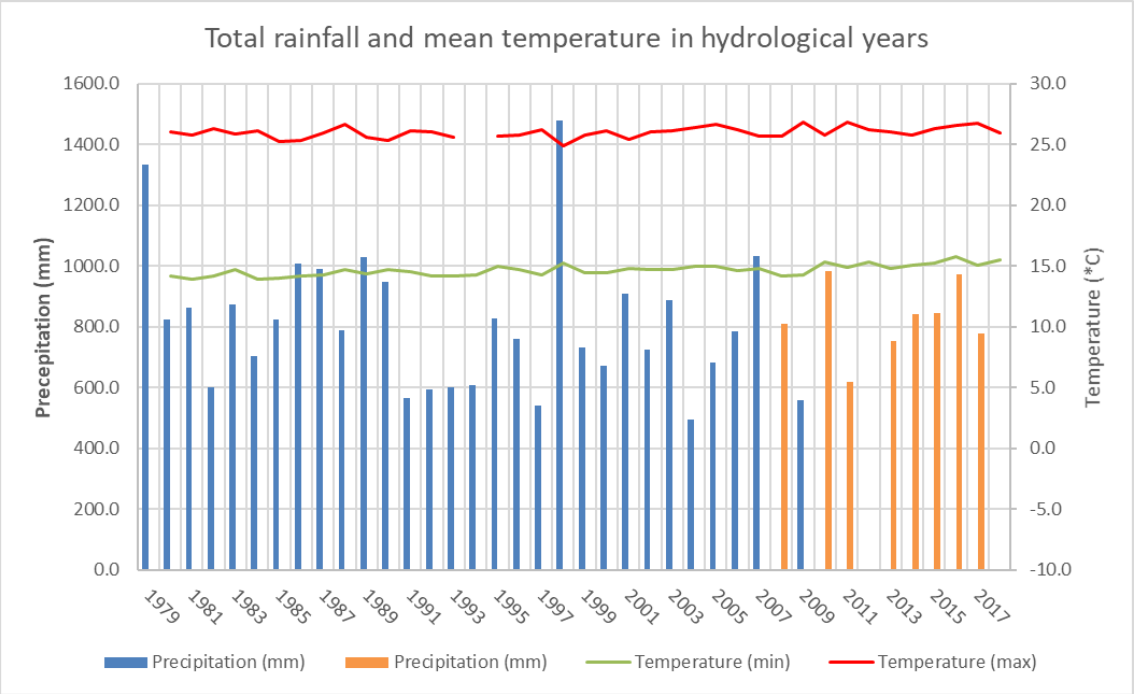

Figure 4: Long term precipitation and min and max temperature. The blue bars represent the precipitation averaged over the three available meteostations, the orange bars represent the precipitation computed from available data supplemented with monthly averaged precipitation.

African Rift System (EARS). The lake is shallow and saline, and is situated 960 m a.s.l. The lake varies in extend between 410 and 480 km^2, and has also dried up in the past completely during dry seasons.

In the districts are multiple large volcanic mountains, both active and inactive. These mountains stand out in the dominantly flatter landscape, and often have higher rainfall on or near their slopes. Apart from the forests on the slopes of the mountains savannah is the major land cover type. Savannah are grasslands, which also have trees and shrubs. Savannah's are generally on the transition area between tropical rain forests to deserts, which in this area is represented by the forests of the Monduli mountains, Mt. Meru and the Ngorongoro, and the drier more arid regions of Simanjiro District and Dodoma Region in the south. The savannah's might have been maintained and extended by the Maasai through fire and grazing of their livestock, suppressing the growth of bushes and trees.

2.2 Land cover classification

Imagery from the Landsat Thematic Mapper (TM), Landsat Enhanced Thematic Mapper plus (ETM+) and the Landsat Operational Land Imager (OLI) instruments was used to identify and quantify long term LULC change in the study area. Multiple other studies conducted in Tanzania have applied this approach (Msoffe et al., 2011; Mtui et al., 2017). Most of these studies used only two or three images at different time periods to assess the LULC change, which enlarges the possibility of analysing an anomaly due to a bias in data. If errors are made in the assessment of one image, this would have a large influence on the total outcome. Therefore, this study used 32 images made between 1982 to 2018. Landsat images were selected to cover the study area (path 168, row 62 and 63). To ensure the assessment of the selected images would not provide biased information, data of the available monthly rainfall were obtained from the Tanzanian Meteorological Agency

(TMA). The amount of rainfall strongly limits the vegetation cover in semi-arid countries, so this information is important to determine about the likelihood of biased classification.

Landsat missions have created the longest continuously-acquired data archive of the Earth surface. The images were obtained from the United States Geological Survey (USGS) through the Google Earth Engine (GEE) workspace (Gorelick et al., 2017). Data from the Landsat 4, 5, 7 and 8 satellites were chosen for this study due to their coverage since 1982 and collection of medium resolution (30 m) multispectral images. All images from Landsat 4, 5 and 8 in the time period 1982 to 2019 covering the study area were selected. The imagery was pre-processed to convert the raw scenes to at-sensor reflectance for accounting of the solar elevation and the seasonally variable Earth-Sun distance. Images taken on the same date were mosaiced to cover the whole research area in every image. The images with less than 10% cloud cover over the research area were selected and clouds were masked with a rudimentary cloud scoring algorithm provided by GEE.

The classification and analysis of the LULC classes was done with the GEE workspace. This is a high-performance computing platform which gives access to a vast and expanding amount of (pre-processed) earth observation data. Moreover, it enables storage, processing and the analysis of big datasets without being expensive or time consuming.

To model and predict the LULC classes, the Random Forest classification algorithm was used in GEE. This is a pixel based decision tree classification algorithm. Decision tree classification algorithms have been widely used for different image analysis and classifications (Midekisa et al., 2017) and have proved to improve the classification accuracy (Gislason et al., 2006).

The overall accuracy of the image classification will be strongly influenced by the selected training properties and the training data (Millard and Richardson, 2015). For the training and classification multiple spectral bands were used (blue, green, red, Near infrared (NIR), two Shortwave infrared bands (SWIR1/SWIR2), NDVI and NDWI (Table A.1/A.2). The NDVI is an indicator of the vitality and density of vegetation at a pixel (eq. 1). The NDWI is an indicator of the presence or absence of water in waterbodies using green and NIR wavelengths (eq. 2).

$$NDVI = \frac{\rho_{NIR} - \rho_{Red}}{\rho_{NIR} + \rho_{Red}} \tag{1}$$

$$NDWI = \frac{\rho_{green} - \rho_{NIR}}{\rho_{green} + \rho_{NIR}} \tag{2}$$

where rho (ρ) is the surface reflectance (-). The NDVI is based on different intensities of reflected sunlight from the visible and near infrared (NIR) part of the electromagnetic spectrum (400-700 nm and 700-1100 nm, respectively). Healthy plant leaves will mostly absorb light from the red spectrum (630-690 nm) and will re-emit radiation from the NIR part of the spectrum because the energy is too large to synthesize. The NDVI ranges from -1 to +1. NDVI values below 0 indicate the presence of water, up to 0.1 indicate rock, sand and snow, 0.2 to 0.3 represents shrub and grasslands, while high values (0.6 to 0.8) indicate temperate and tropical rainforests.

To increase the accuracy the properties elevation and slope of the surface were also added. The elevation and slope surface were derived from data of the Shuttle Radar Topography Mission (SRTMGL1v3), which was re-sampled to a resolution of 30 m. This resulted in a total of 10 properties to train on.

Improvement of the classifier

The algorithm performing the classification had to be trained. The resulting classifier was tested on performance accuracy. To increase the accuracy and reliability of the outcome

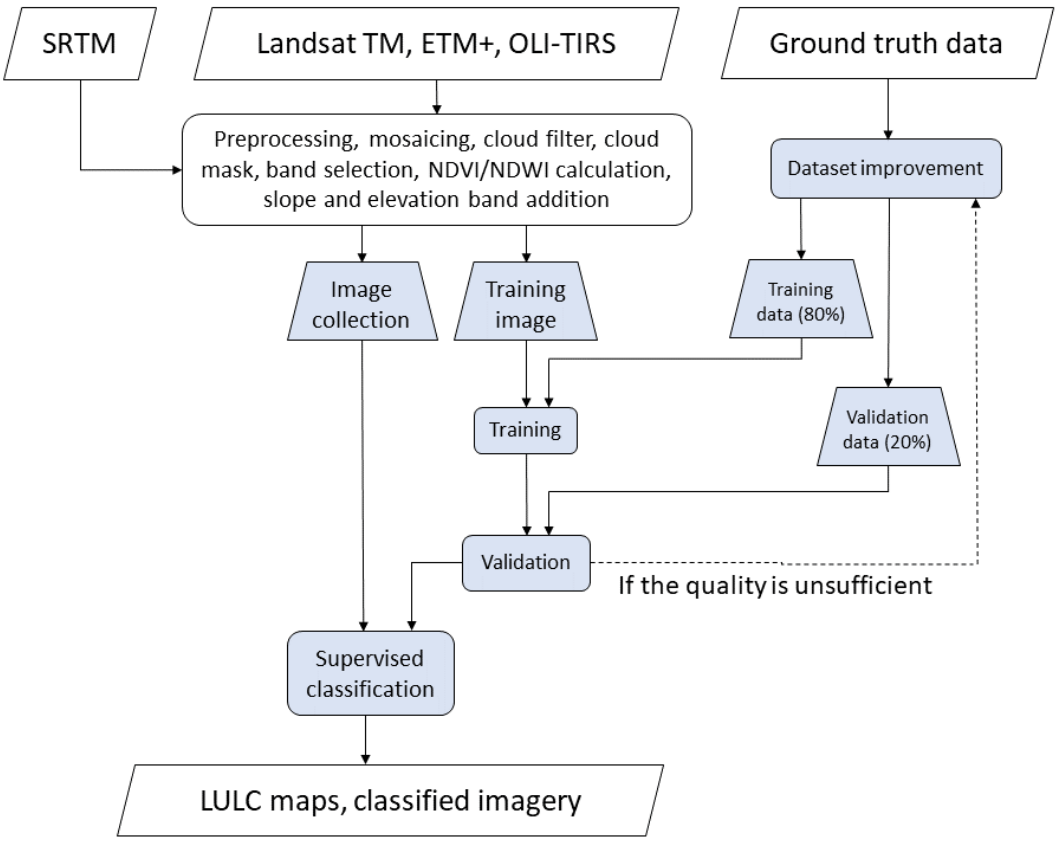

Figure 5: Flow chart of the LULC classification. Blue boxes consist out of a separate flow for a classification of imagery from the dry or the wet season

three steps were undertaken. First the dataset for training and validation[1] was adjusted. This included the aggregation and splitting of LULC classes and addition and exclusion of data. The addition and exclusion were done on the basis of local knowledge and high-resolution satellite imagery. Secondly the images used for training were changed from one to two for the different seasons. Thirdly the used bands for training and classification were tested for an in- or decrease of the accuracy. The accuracy of the training properties has been tested with all properties but one left out to check if any band would contribute negatively to the accuracy.

The dataset consisted out of approximately 150 polygons of ten selected classes (Table 1, Figure 6). The data in the dataset was collected during a ground survey in the first quarter of 2019 and supplemented based on high resolution satellite imagery and local knowledge. The classification is based on the land-cover definitions used by the International Geosphere-Biosphere Program (IGBP) (Loveland and Belward, 1997). The original dataset has 3019 pixels, both for training and validation. The datapoints were collected in Monduli District and neighbouring Karatu district and were chosen on accessibility and homogeneity of the land cover class. The data points of the training datasets should be randomly distributed or have a proportional amount of data of each LULC class (Millard and Richardson, 2015). Since the acquisition of data points was largely dependent on accessibility the data points were collected proportional according to the LULC distribution determined by Bergh (2016). The dataset for classification was adjusted according to different factors. In order to increase the total accuracy, the dataset was changed nine times. The size of the polygons was changed, polygons were added and polygons were

[1]hereafter training data or dataset unless stated otherwise

Table 1: Land-use and land-cover classification scheme. Adopted from Loveland and Belward (1997)

Class	Class name	Description
5	Mixed forests	Land dominated by trees >2 meters and a canopy cover >60%. Consists of tree communities with interspersed mixtures or mosaics.
6	Closed shrubland	Land with woody vegetation (evergreen or deciduous) <2 meters tall and with shrub canopy cover >60%.
7	Open shrubland	Lands with woody vegetation (evergreen or deciduous) <2 meters tall and with shrub canopy cover between 10-60%.
8	Woody savannah	Lands with grasses, forbs and other understory systems, with canopy cover between 30 and 60% (evergreen or deciduous). Tree height >2 meters
9	Savannah	Lands with grasses, forbs, and other understory systems and with tree canopy cover between 10% and 30% Tree height >2 meters.
10	Grassland	Lands with variety of grasses and forbs. Woody vegetation cover (trees and shrubs) is less than 10%.
12	Agriculture	Lands covered with temporary crops followed by harvest and bare-soil period e.g. single and multiple cropping systems. Perennial woody crops are classified as the appropriate shrubland cover type.
13	Built up / natural vegetation mosaic	Lands with houses at least 40%, and 60% composed of natural vegetation (trees, shrubs grass, forbs), bare land (rock, soils or sand) (modified definition).
16	Barren or sparsely vegetated	Lands with exposed soils, sand or rocks, with no more than 10% vegetation cover at any time of the year.
17	Water bodies	Lakes, streams, rivers and water holes (boreholes).

deleted from the dataset. This had an effect on the total amount of pixels in the dataset and also on the amount of pixels per class (Table 2).

Training imagery

The classifier was trained with the use of satellite imagery. For the training two different sets of imagery were used for the different sensor types of the satellites. The bands from the TM and ETM+ sensors have the same bandwidth (Table A.1), however the OLI sensor from Landsat 8 is slightly different (Table A.2). Therefore the training of the RandomForest algorithm was done with seperate images of Landsat 7 and Landsat 8.

Furthermore, with the use of the first 5 datasets only one pair of images was used

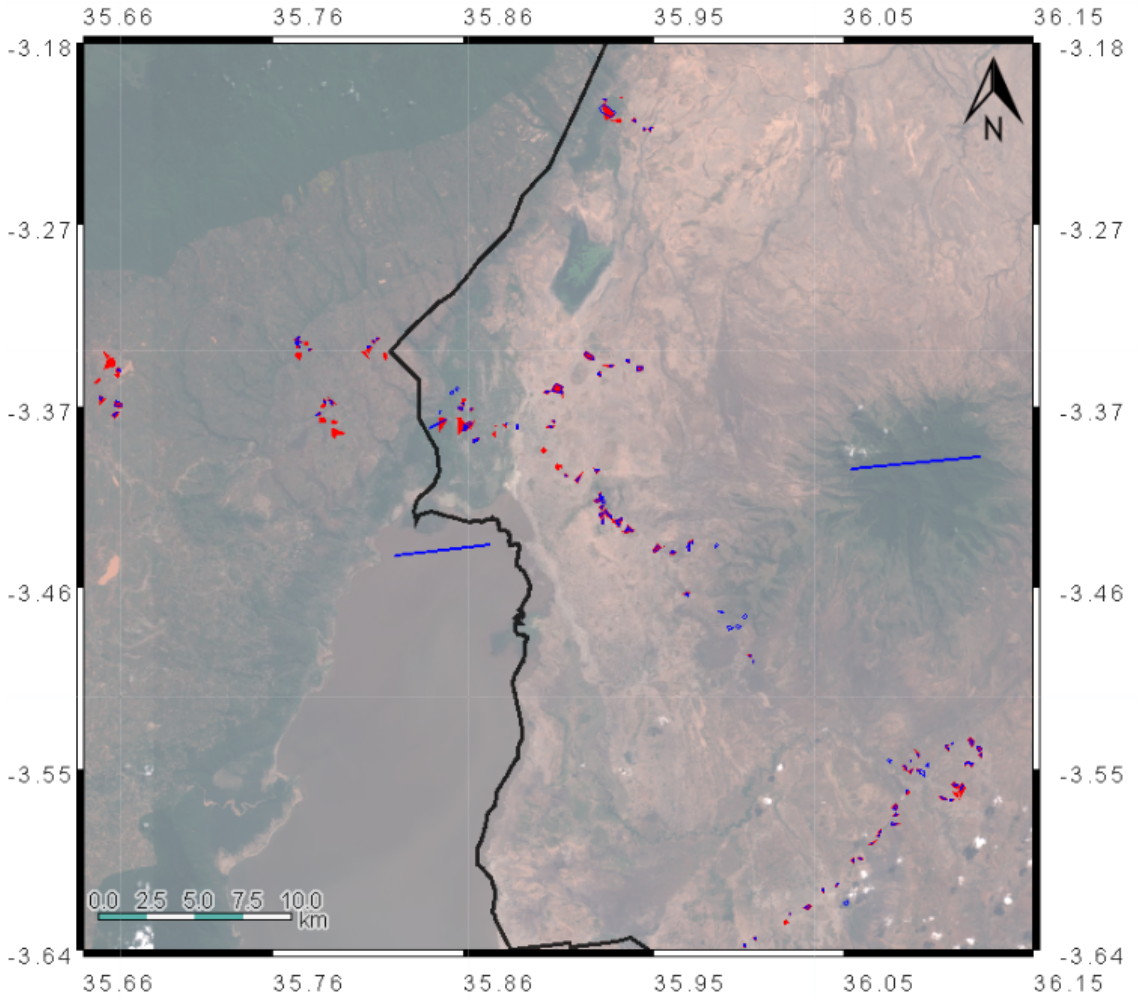

Figure 6: Satellite image with the locations of the training and validation dataset. In red are the locations of the data from dataset 1, blue are the locations of the data from dataset 6.
Source: https://code.earthengine.google.com/65bf716f8bfa8c0b3aa8d94fdf198582.

for the training. Those images were selected on cloud cover and to match the date of acquisition with the date of ground truth data collection (Q1 2019, wet season). In the training with dataset 6 a distinction was made between the dry and wet season. Due to a high variability of the phenology of vegetation in semi-arid and arid landscapes it was chosen to make a second classifier based on images of the dry season and to classify images of the dry season. All pixels of the dataset were (visually) corrected for notable errors of classification during the dry season, and a second set of training images was chosen which were cloud free and obtained during the most recent dry season (Table B.1). Due to a defect in the Scan Line Detector datagaps exist in Landsat 7 imagery. This caused a part of the training data to be unusable with the Landsat 7 imagery (16%).

LULC classification validation

The classification of the landscape has been performed with the three changing input parameters: the training data, the training images, and the LULC classes. For the training of the classifier a randomly selected eighty percent of the dataset was used. The remaining twenty percent was used for validation and describing the performance of the classification model (Xiong et al., 2016). A confusion matrix was created, together with the user's (A_u), producer's (A_p), and overall (A_o) accuracies and the Kappa coefficient ($\hat{k}$), which

Table 2: The amount of pixels per class and total per training dataset.
Source: https://code.earthengine.google.com/fcead8006a7d38f45804094719365c52

Class	Description	Dataset 1	2	3	4	5	6 (rainy)	6 (dry)
5	Forest	506	1507	506	2062	24432	759	759
6	Closed Shrub	31	31	31	29	29	30	30
7	Open shrub	86	86	86	64	60	63	63
8	Woody savannah	193	193	193	215	215	429	429
9	Savannah	232	232	262	218	218	197	197
10	Grassland	587	587	587	557	557	566	566
12	Cropland	867	779	294	244	244	513	368
13	Urban	352	247					
16	Bare	94	94	94	99	99	106	113
17	Water	71	1071	1071	1071	1071	244	373
50	Dry broadleaf					109	157	154
	Total	3019	4827	3124	4559	27034	3065	3053

are given by:

$$A_o = \frac{S_d}{n} \tag{3}$$

$$A_u = \frac{X_{ij}}{X_j} \tag{4}$$

$$A_p = \frac{X_{ij}}{X_i} \tag{5}$$

$$\hat{k} = \frac{A_o - A_e}{1 - A_e} \tag{6}$$

in which

$$A_e = \frac{1}{n} \sum_{i=1}^{r} x_{i+} \cdot x_{+i} \tag{7}$$

where S_d is the total number of correct classified pixels, n is the total number of pixels, X_{ij} is the observation in row i column j, X_i it the marginal total of row i, X_j is the marginal total of column j, x_{i+} is the marginal sum of row i, and x_{+i} is the marginal sum of column i. Kappa is a useful measure of classification accuracy, because it compensates partly for the low number of classes which might produce a high accuracy because of the simpler legend (Xiong et al., 2016; Rossiter, 2014). The accuracies, interpretation of imagery and field experience was used to determine the overall reliability of the results. The LULC classifications resulted in LULC maps of which the area per class was computed. This resulted in a class area change over time.

2.3 Seasonal vegetation dynamics

NDVI is regarded as a reliable indicator for land cover conditions and variations, and over the years it has been widely used for vegetation monitoring (Lanorte et al., 2015). By measuring the NDVI the canopy 'greenness' of the system will be determined during different seasons. It has been shown to be closely associated with other qualitative vegetation parameters, such as canopy cover, leaf area index and biomass (Xie et al., 2016).

Based on the results of the LULC classification, medium and high resolution imagery and local knowledge eight groups representative for the dominant vegetation types were located (Table E.1). Each group consisted out of one or more areas, of which the average

NDVI was calculated. For each location a dataset was made with images covering the area with no cloud cover.

Dataset

Images from Landsat programmes 4, 5, 7 and 8 were used. The bandwidth of the sensors is different for each instrument (Table A.1/A.2), resulting in differences in the vegetation index. If the NDVI from different instruments is compared, they vary a few percent, but the values were shown to be highly linearly correlated (She et al., 2015; Roy et al., 2016; Ju and Masek, 2016; Steven et al., 2003). This enables the calibration of NDVI between the different sensors. The Landsat 4 and 5 TM sensor was not corrected because it has similar responses as the 7 ETM+ sensor (Steven et al., 2003) and has too limited data in the areas to produce significant correction factors (Table E.2).

An ordinary least-squares linear regression was used to correct the OLI-TIRS data to TM/ETM+ data. The dataset used for the correction factor consisted out of images from different satellites but taken on the same date, 1 day or 8 day difference (Ju and Masek, 2016, Appenndix A). A variation in vegetation of the eight areas results in the generation of different NDVIs (She et al., 2015). Therefore for each location a correction factor was computed between the TM/ETM+ sensor and the OLI-TIRS sensor. If R^2>0.40, the slope of the regression line was used as the correcting factor, else no correction factor was used (Table 3).

The Landsat at sensor imagery was pre-processed, consisting of amongst other things atmospheric correction and computation of the cloud/shadow pixels (Zhu et al., 2015). Clouds and aerosols were masked out of the surface reflectance imagery with the use of the pixel_qa band.

Trend analysis

The dataset of each location consisted of 362 up to 756 images, depending on the exact locations chosen. The temporal dispersion within the datasets was based on the availability of cloud free images. This resulted in on average 6% of the images being made between 1985 and 2000, and the remaining 94% between 2000 to 2019 (Table E.2).

The NDVI can be distorted by undetected cloud or cirrus cover, or shadows in the imagery. Therefore monthly averaged values were used if multiple NDVI values were available. With these monthly averaged values seasonally averaged NDVI values were derived for the wet season (FMAM), dry season (ASO) and annual values (Aug-Jul).

Due to the non-normal distribution of data over time the Mann Kendall (MK) trend test was chosen to identify of any long-term trend in the NDVI. The MK is a non-paramteric rank-based test method which is widely used to assess the presence of any trends in a

Table 3: Correction factors of the OLI-TIRS NDVI values for each area in the form $Y = a \cdot x + b$. If $R^2 \leq 0.4$ the correction factor was not applied and the original values were used. The $Date\Delta$ is the difference in date of the paired NDVI of TM/ETM+ and OLI-TIRS imagery. Positive values represent OLI-TIRS imagery to be later taken, negative values represent OLI-TIRS imagery to be earlier taken than the corresponding TM/ETM+ imagery

	Grass N	Grass S	Forest	Sav. N	Sav. S	Rice	Banana	Intercrop
a	0.7766	0.9062	*-0.0003*	0.9035	0.8341	0.533	*0.2556*	1.0248
b	-0.0104	-0.0445	*0.7842*	-0.0415	-0.0158	- 0.3275	*0.4512*	0.1019
R^2	0.771	0.769	*2.00E-07*	0.743	0.643	0.593	*0.069*	0.551
r	0.878	0.877	0.000	0.862	0.802	0.770	0.263	0.742
Date Δ	+8	+1	+1	+8	+1	+1	+1	-1

time series of climatic data, environmental data, or hydrological data (Teferi et al., 2015; Mbatha and Xulu, 2018; Nasanbat et al., 2018; Chamaille-Jammes et al., 2006; Forkel et al., 2013). The MK is calculated by:

$$S = \sum_{k=1}^{n-1} \sum_{j=k+1}^{n} sign(X_j - X_k) \tag{8}$$

$$sign(X_j - X_k) = \begin{cases} +1, & if \quad (X_j - X_k) > 1 \\ 0, & if \quad (X_j - X_k) = 0 \\ -1, & if \quad (X_j - X_k) < 1 \end{cases} \tag{9}$$

$$Var(S) = \frac{1}{18}\left[n(n-1)(2n+5) - \sum_{p=1}^{q} t_p(t_p-1)(2t_p+5)\right] \tag{10}$$

$$Z_{MK} = \begin{cases} \frac{S-1}{\sqrt{Var(S)}} & if \quad S > 0 \\ 0 & if \quad S = 0 \\ \frac{S+1}{\sqrt{Var(S)}} & if \quad S < 0 \end{cases} \tag{11}$$

where $sign$ is the signum function, X_i and X_j are the sequential data values of the time series in the years i and j, n is the length of the time series, t_p is the number of ties for the p^{th} value, and q is the number of tied values. Positive values of Z_{MK} indicate increasing trends, while negative Z_{MK} values indicate decreasing trends in the time series. The value of the S statistic is associated with the Kendall's tau (τ):

$$\tau = \frac{S}{D} \tag{12}$$

$$D = \left[\frac{1}{2}n(n-1) - \frac{1}{2}\sum_{p=1}^{q} t_p(t_p-1)\right]^{1/2}\left[\frac{1}{2}n(n-1)\right]^{1/2} \tag{13}$$

where D is the denominator (-). The MK was applied on the seasonal and yearly NDVI per area. The value of τ correlation indicated the strength of the trend if the trend was significant. Another correlation coëfficient for ordinal data would be Spearman's Rho (ρ), but ρ is less reliable with many ties in the dataset.

The intra-annual variability and resilience of the areas to drought was tested with the use of the corrected NDVI values from the Landsat 4, 5, 7 and 8 satellite. Of each datapoint the day of year (DOY) was computed and plotted against the NDVI values. In order to test for drought on the vegetation the NDVI values were divided in three groups, based on the amount of precipitation of the hydrological year. The meteorological station at Karatu has the longest record of annual precipitation (TMA, 2019), therefore this record was used to test for the first and third quartile of annual precipitation which resulted in 714 mm and 950 mm. Each group of NDVI values (dry, normal or wet year) was tested with the use of local regression (LOESS). To test for the resilience of the systems two groups were added, with respectively the NDVI values the first, and the second year following after a dry year. The different agricultural areas were not tested with the data of the second year following after a dry year due to the high anthropogenic influences on the system and the effect of this on the vegetation.

Climatic factors

The health of vegetation and NDVI is dependent on many anthropogenic and natural factors. The most important natural factors are temperature and precipitation (Moulin

et al., 1997). Because water is the most limiting factor for vegetation growth in semi-arid systems, the NDVI is compared to the response to precipitation. Long term monthly precipitation measurements (1968-2018) and short term daily precipitation (2009-2014) were recorded (TMA, 2019). Data from three stations close to the research area (Karatu, Babati and Monduli) was used and the monthly rainfall were all well correlated (τ>0.64, Z>17, p<$2.2E^{-16}$). The precipitation of the area was obtained by calculating the mean monthly average of at least two stations. The seasonal (wet and dry) and yearly precipitation (hydrological year: Aug-Jul) was tested for any monotonic trends with the use of MK. The correlation between the intra-annual precipitation and NDVI of the different areas was tested with Kendalls tau (τ). The long term annual NDVI and precipitation was not tested due to the little overlap in data and the data gaps present in the NDVI dataset. A dataset of long term monthly minimum and maximum temperature (1980-2018) was also tested with MK. These results were used for better interpretation of the results of the trend analysis on the NDVI.

2.4 Local perspective on environmental change

In addition interviews were held with local inhabitants. This gave an insight on the perception of LULC change, vegetation dynamics and climatic variations. In total 16 households from three villages were interviewed with the use of one or two (local) translators (Kiswahili and Maasai languages). The selection of interviewees was based on accessibility, willingness to participate and the participation in agro-pastoralism because of the higher dependency on the climate and environment. Both men and women were involved, although the majority of respondents were men. The reason might be that women may have been reluctant to be involved in the interviews due to cultural standards. The questions used for the survey were semistructured, which helped to derive qualitative and quantitative information. It was designed to retrieve information on (1) the respondents social, economic and geographic characteristics (livestock holdings, land ownership, income sources); and (2) experiences on (a) vegetation health and dynamics, and (b) climatic factors and water availability. The results of the interviews were used to put the LULC change and vegetation dynamics in perspective.

3 Results

3.1 LULC change

The collection of images for the analyis of LULC change resulted in a series of images covering 98% of the study area. Due to the flight plan of the satellites an area in the north-west (the Ol Doinyo Lengai vulcano) is not included in the imagery. The images including this area could have been mosaiced to the images for analysis, but the acquisition date and time will be different which would result in a deviating classification of this area. An area of approximately 275 km^2 is therefore not included.

The image collection comprises 32 images with a different acquisition date (Table B.2). The maximum cloud cover of these images over the research area is 9.90%, with an average of 3.75%. This set comprised of 7 images from the Landsat 4/5 satellite in the period between January 1985 and November 2009, and 25 images retrieved from the Landsat 8 satellite acquired between August 2013 and March 2019. This resulted in a coarse temporal resolution for the first thirty years and a relatively fine temporal resolution for the last six years.

Improvement of the classifier

Six important datasets with the ground truth and training data were used:

1. The first classifier was made with the collected data with ten different classes (Dataset 1). The accuracy of the classifier was high (0.92) but the classified LULC maps were unrealistic (Figure D.1/D.2). The classes shrubland and savannah were merged because of the low representation of these classes, their similarity and to increase the reliability of the classification of this class (John et al., 2009). However, the unrealistic results of urban, forest, agriculture and water area led to the rejection of the results.
2. To increase the accuracy of urban, water and forested areas pixels were added to the second dataset. By adding data, the spectral range of these classes would be more accurately represented. With a correct spectral representation of the training data the classifier would be improved. Therefore two areas were removed because these contained too many contaminated pixels (pixels assigned to a class while representing another class). This resulted in a over estimation of agricultural lands and a still highly fluctuating forest area through the seasons. Thus these results were rejected.
3. With only connecting roads and no big cities or towns in the research area the relative appearance of urban area is small. This information, together with the doubtfull results of urban classification the urban class and training data was excluded for this and further datasets. The class agriculture showed to be unlikely widespread and to have a similar pattern with bare area from Bergh (2016), so the data was checked for contamination with the class bare. The dataset was checked and suspected contaminating pixels were excluded. The dataset was also expanded with some water (like dataset 2) and new agricultural areas. This resulted in a extremely varying total size of forest area (Figure D.4c/D.4d) and to a lesser degree bare area. The implausibility of fast growth and deforestation caused the rejection of these results.
4. Dataset 4 and 5 were focussed on solving the big (seasonal) variation in total forest area (Figure 7). By adding respectively 1500 and 24000 training pixels of forest, the aim of a perfect spectral representation of forest was tried to be approached. However, the dataset should have a proportional amount of pixels attributed to each

class. Due to the impossibility of adding a similar proportional amount of pixels from other classes, an overestimation of forested area was the result and thus the classification did not improve. For dataset 5 a distinction was made between moist and dry (sub)tropical broadleaf forest. The moist (sub)tropical forest was assumed to be less rainfall dependent and to be evergreen. The dry (sub)tropical forest was characterized by forest of thorny trees and shrubs such as acacia. The expansion and decrease of forest could have been caused by the correct and incorrect classification of the dry (sub)tropical forest. Due to its decrease in leaf area in the dry season and corresponding canopy, the see-through from space is enhanced resulting in increased soil detection. This was not successful in the training and did not result in a more continuous surface area of moist (sub)tropical forest (Figure D.6c). The tested accuracy of dataset 5 is on average the highest (0.994) which can be attributed to the high amount of forest training pixels (Table 2). The high amount of pixels in one class results in a high producers accuracy for that class but the producers accuracy for the other classes remain relatively low (Table C.1 and C.2). The accuracy is therefore not useful. Yet again, the results were rejected.

6. The strong spectral difference of vegetation during the year resulted in a big variation of classifications. By changing the classification into a dual dataset and classifier, this effect was attempted to decrease. The dataset was duplicated into one for the dry classifier and one for the wet classifier. The amount of pixels from forest and water were restored to reasonable levels (compared to dataset 5). All pixels for both datasets were visually checked for applicability and contamination with the use of imagery from both the wet and dry season.

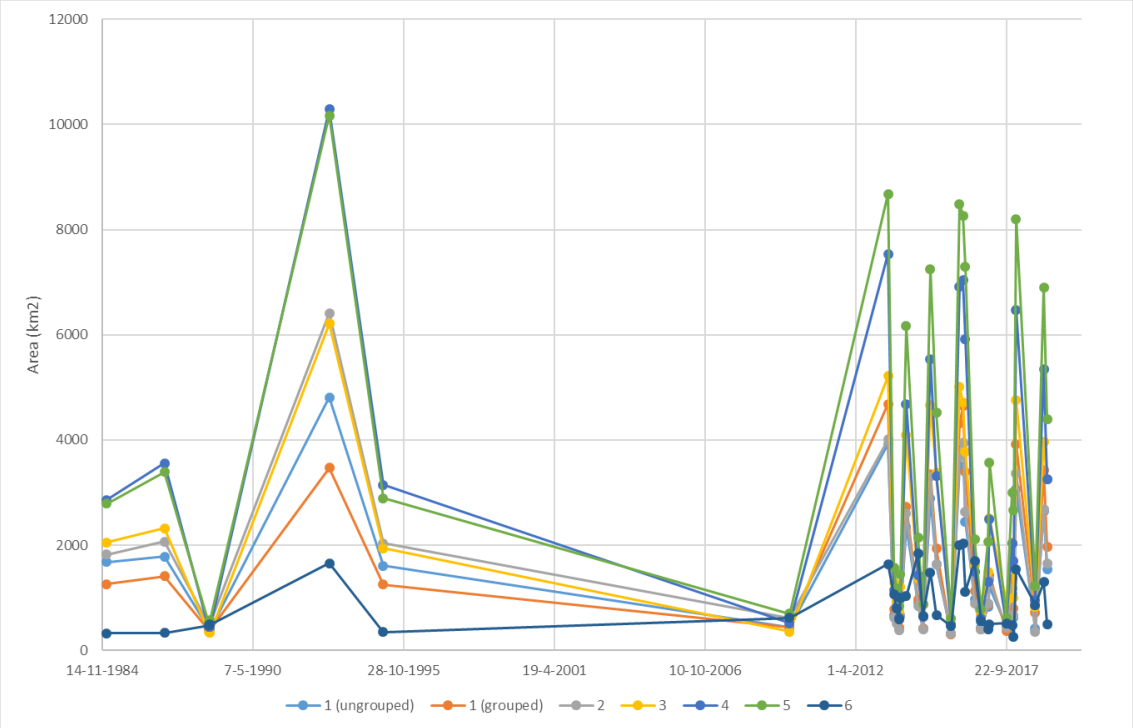

Figure 7: Area of the class forest over time and based on different training datasets

The adjustment of the dataset for training and validation increased the accuracy on average from 0.92 to 0.96 (Table 4 and Table C.3 to C.6). The accuracy of dataset 5 is on average the highest (0.994) which can be attributed to the high amount of pixels in class 5, forest (Table 2). The high amount of pixels in one class results in a high producers

accuracy for that class but the producers accuracy for the other classes remain relatively low (Table C.1/C.2). The kappa index is between 0.93 and 0.96 for the four training images of the last dataset.

The changes in the dataset and different training images had an effect on the classification algorithm. This resulted in different classifications of satellite imagery (Fig D.1 to D.6). In figure 8 the LULC class size on 29 January 2018 can be seen, resulting from the different datasets. This date was chosen because it is close to and in the same season as the training images. It can be seen that the changes of the dataset had a big influence on the classification area. The class urban showed a relatively high area in the first datasets, which was one of the reasons to exclude this class in the next datasets. The class forest showed an overestimation of the total area for almost all of the datasets when this was visually compared with true- and false-color imagery. The class savannah has increased at least twice in dataset 6 for this date.

In image 7 the area size of the class forest is depicted over time. The total classified area forest fluctuates a lot over time and also between the different datasets. The trend of each dataset is similar, with some exceptions for dataset 6. This is caused by the difference of the training images used for the classifier. For datasets 1-5 only one image was used for training, originating from the wet season (21 Mar 2019), and for dataset 6 this was changed to two training images and classifiers for both the wet and dry season. This resulted in a totally different classifier for the images of the dry season.

A strong seasonal periodicity of the area sizes would result in a specific trend throughout the year. In Figure 9 the area size of the classes is measured for the day of the year

Table 4: The accuracies of the training based on different datasets. Grouped and ungrouped refers to the grouping of the savannah class (class 6, 7, 8 and 9).

	Landsat 7		Landsat 8	
Dataset	Wet	Dry	Wet	Dry
1 (ungrouped)	0.915	0.915	0.916	0.916
1 (grouped)	0.923	0.923	0.924	0.924
2	0.960	0.960	0.941	0.941
3	0.940	0.940	0.940	0.940
4	0.969	0.969	0.976	0.976
5	0.995	0.995	0.994	0.994
6	0.955	0.970	0.966	0.950

Table 5: Accuracies of the used properties for the training based on Trainingset 6.

	Landsat 7		Landsat 8	
Property left out	Wet	Dry	Wet	Dry
None	0.955	0.970	0.966	0.950
Blue	0.941	0.958	0.958	0.954
Green	0.943	0.962	0.958	0.951
Red	0.957	0.956	0.972	0.953
NIR	0.945	0.960	0.969	0.953
SWIR1	0.949	0.958	0.964	0.961
SWIR2	0.955	0.956	0.959	0.943
Elevation	0.941	0.952	0.964	0.950
Slope	0.912	0.935	0.940	0.929
NDWI	0.953	0.956	0.964	0.953
NDVI	0.951	0.966	0.966	0.951

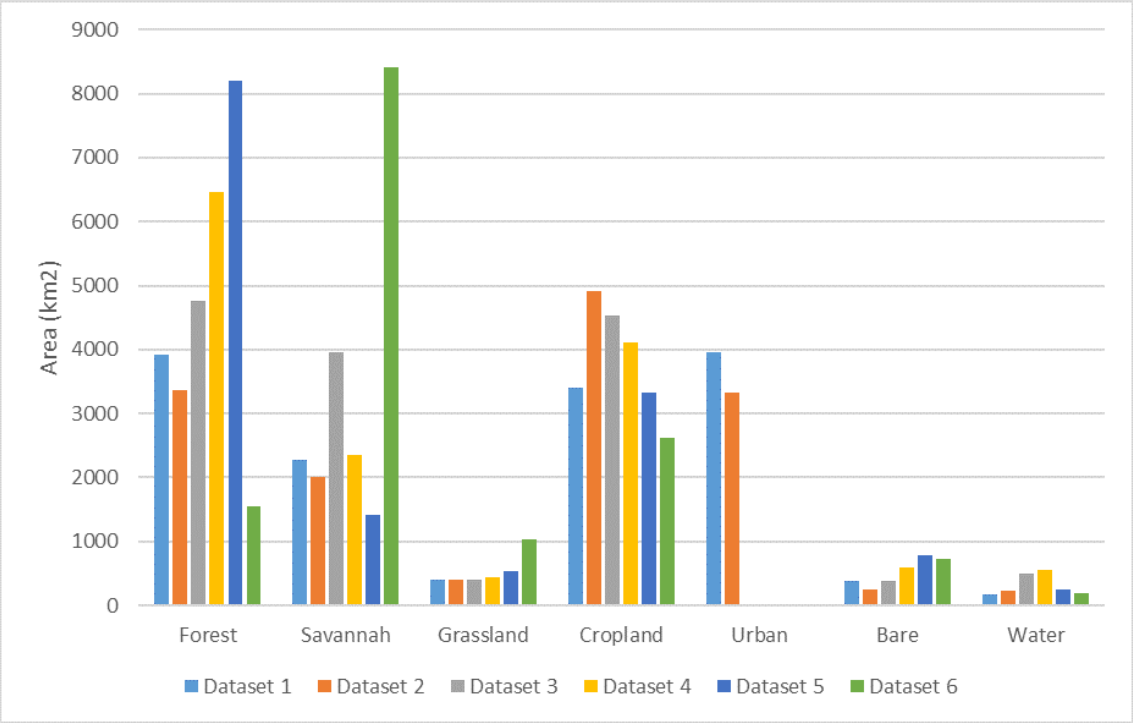

Figure 8: Class sizes on 29th Jan 2018 classified for different datasets.

(DOY). The data originating from the Landsat 4/5 satellite is omitted from this graph to exclude errors originating from the different sensors. All classes have a high variability of area size during a large part of the rainy season (Dec-Mar). During the dry season an increase of grassland and bare soil is observed and a decrease of agriculture and forest.

The area per class over time is shown in Figure 10 and 11. The different satellites used in this research is clearly visible in the graph of Figure 10. The little amount of datapoints (7) between 1985 and 2013 (Landsat 4/5) is in sharp contrast to the relative high amount of datapoints in the timeperiod of 2013-2019 where data of the Landsat 8 was used.

The class savannah is most dominant in the area all the time except for one moment. The classes forest, grass and agriculture cover during the whole time-span the same range of total area of 300 to 3000 km^2. In the years 1985-2010 bare has the second largest area, and after this period it merges with the classes forest, grass and agriculture. Periodicity for many classes can be seen during the period 2013-2019. Savannah shows a drop in the wet season (around February) in 2016, 2017, 2018 and 2019, when many other classes show peaks of area size.

The class water is the least abundant in the area but also shows some peaks around the wet seasons between 2014 and 2019. Cloud shadows were not masked in the images and were often classified as water. The increase of water is mostly close to Lake Natron in the north-west just outside the study area. Flooding of this lake could also be the cause of an increase of water.

Bare soil can be dominantly found in the center of the study area surrounding a mountain and spreading to the east (Figure 11). Cropland can be found along the edges of different mountains and mostly along the shores of Lake Natron and Lake Manyara to the south-west. Forest concentrates strongly around mountainous areas and extends and disappears from these patches. Savannah is the most abundant land cover class (39-64%) and can together with grasslands be found on the lower lying plains. The classes grass, agriculture and bare tend to alternate. In Fig. 11a it is mostly classified as bare soil, in Fig. 11b this has been replaced mainly by grassland, while in Fig. 11c it is labelled as

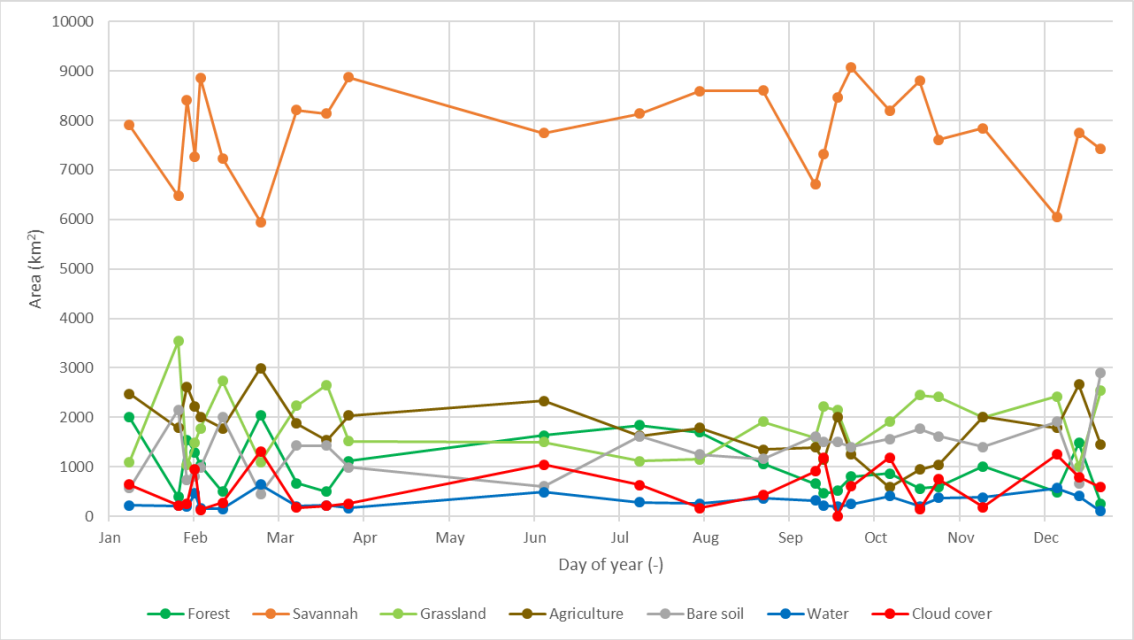

Figure 9: Day of year (DOY) of the class area size of the all available images from the Landsat 8 collection, based on dataset 6.

agricultural area. In Fig. 11d a mix of those three classes is present in the specific area.

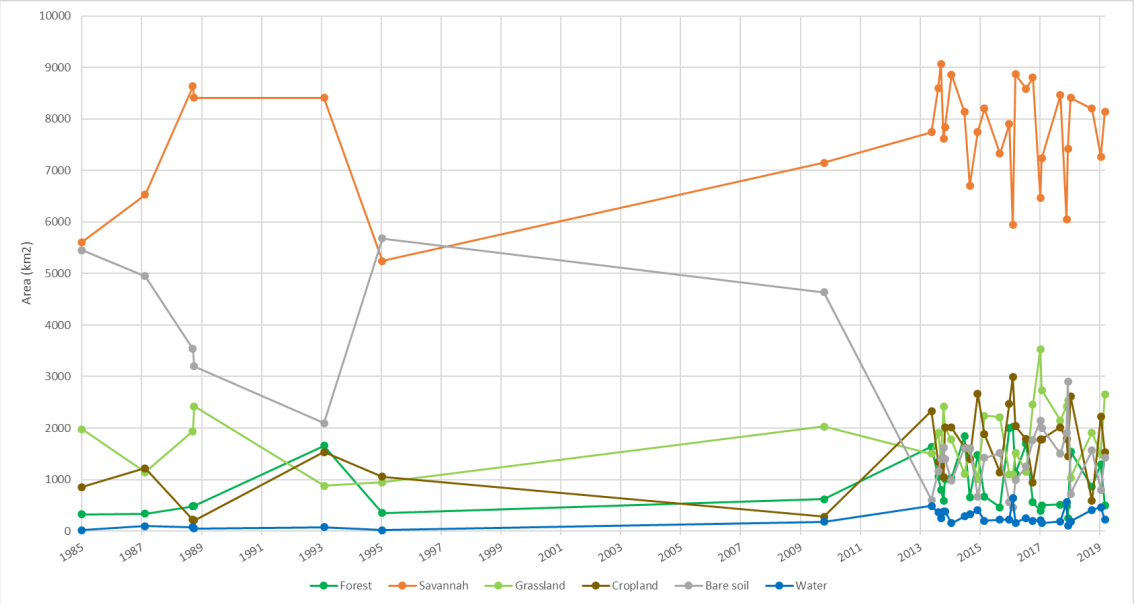

Figure 10: Area of the classes over time based on dataset 6.

3.2 Vegetation dynamics

The effects of droughts and seasonal rainfall on the resilience of the classes in the area was assessed by comparing precipitation data with the NDVI time-series. Trend analysis was applied on the NDVI time-series.

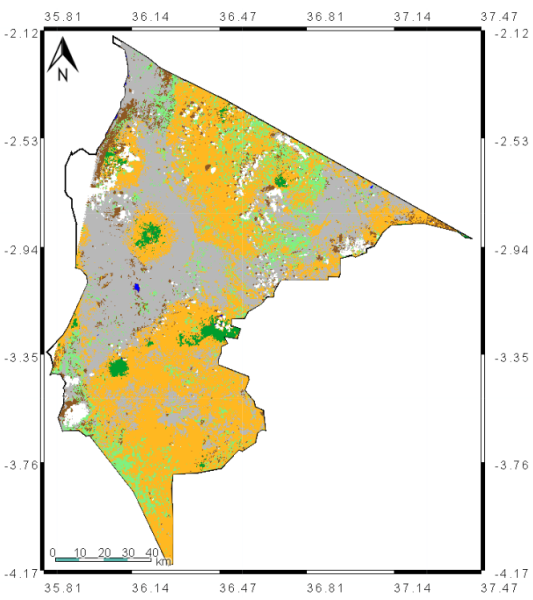

(a) 18 Jan 1985 (wet season)

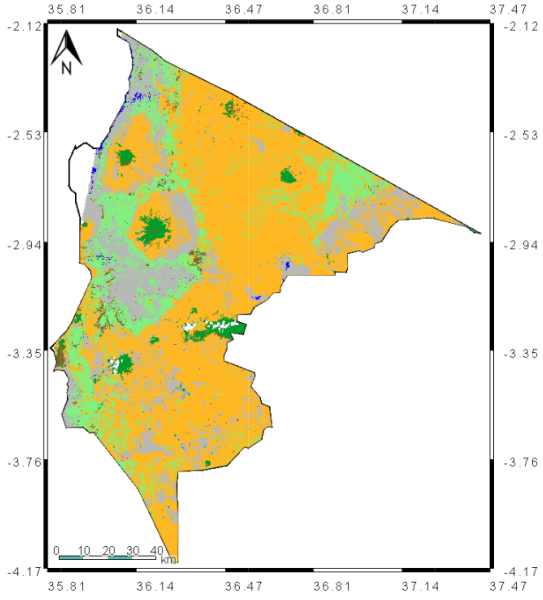

(b) 17 Oct 1988 (dry season)

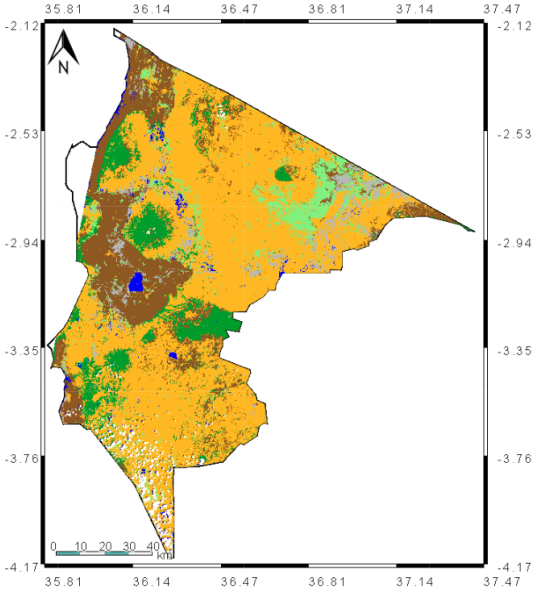

(c) 29 Jan 2018 (wet season)

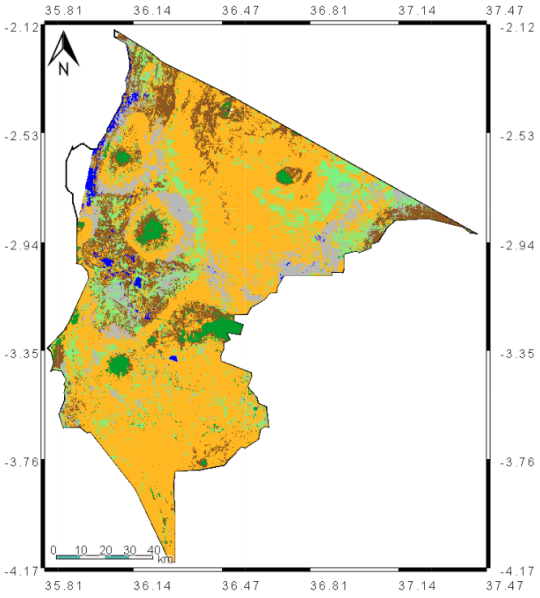

(d) 23 Sep 2017 (dry season)

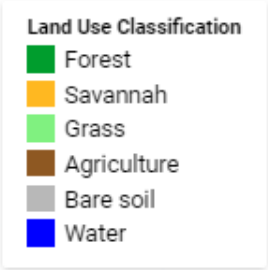

(e) Legend

Figure 11: Land cover maps based on dataset 6.
Source: https://code.earthengine.google.com/3c45bd93284b0b2048cf2bc21d4176ef

Climatic context

The yearly averaged rainfall in the period 1973 to 2009 is 786 mm, with the precipitation having a distinct dry and wet season. The intra-annual variability is very high (CV=94.98%). Of the three meteostations only one siginificant trend was measured. In Karatu there is a negative trend of the rainfall during the long rainy season (MAM)(τ=-0.239, p=0.033)(Table F.1 - F.4). The monthly averaged precipitation over the area shows no significant trends during any season (long dry/wet, short dry/wet, annual).

The yearly averaged temperature in the research area, represented by one meteostation in Arusha, is significantly increasing (all p$<$0.021). Both the minimum and the maximum show a strong positive trend (τ=0.569 and τ=0.262)(Table F.5).

Temporal NDVI-rainfall relationships

In the different areas the NDVI have similar trends during the year, with an increasing NDVI during the wet season and decreasing NDVI during the wet season (Figure 12). The values vary from area to area, and also the range of NDVI differs between the different vegetation types (mean: 0.154$<$NDVI$<$0.687; and variation: 10.18%$<$CV$<$33.86%)(Table E.3). The forested area and banana plantations have the highest and most constant NDVI, while both grassland and savannah have the lowest NDVI values during the dry season (0.10-0.15) and fluctuate more.

The NDVI in all areas except the ricefields is higher during a wet year (Fig. 12, blue line), and lower during a dry year (Fig. 12, yellow line) compared to normal years (green line), and at the end of the dry season (October) the NDVI values of the natural systems return to a steady state in all situations (wet/normal/dry year). The ricefields and agriculture (intercrop) have high NDVI values early in wet season (Nov-Dec) representing the the biannual growth of crops. For the ricefields this is only partially represented by the trendlines due to a smaller amount of data available after the building of an irrigation system in 2012.

After a dry year the response in the south during the first part of the rainy season (Nov-Dec) is similar to the increase in NDVI during a wet year, but at the end of the rainy season it is below a normal year. In the north the response after a dry year is similar to a normal year, which is continued throughout the rest of the wet season. The grasslands in the north have a lag in the decline of NDVI during the dry season which is accompanied with a lack of data in the period July and beginning of August. The trend of the NDVI two years after a dry year (Fig. 12, red-dotted line) is similar to the trend of a normally wet year (Fig. 12, green line). The bananafields and intercrop agricultere show a normal response at the start of the wet season, but at the end of the wet season the values are lower than during the dry year. The ricefields have a trend the other way around, with a slow response to the first rainfall and higher than normal NDVI values at the peak of the rainy season

The non-agricultural areas have a significant and strong correlation between NDVI and rainfall with a lag of 1 month (p$<$0.002, $\tau$$>$0.667) (Table E.4). The banana and maize fields also show a strong significant relation, however with a lag of 2 months (p$<$0.01, τ =0.576).

Long term NDVI

The MK test was applied on the average seasonal NDVI per area for the wet and dry season, and yearly averaged NDVI. This resulted in nine significant trends (all $\tau$$>$0.325, p$<$0.05) (Table 6). The forested area, rice, banana and intercrop fields showed a significant increase of the NDVI over time for both the wet season and annual average. The banana

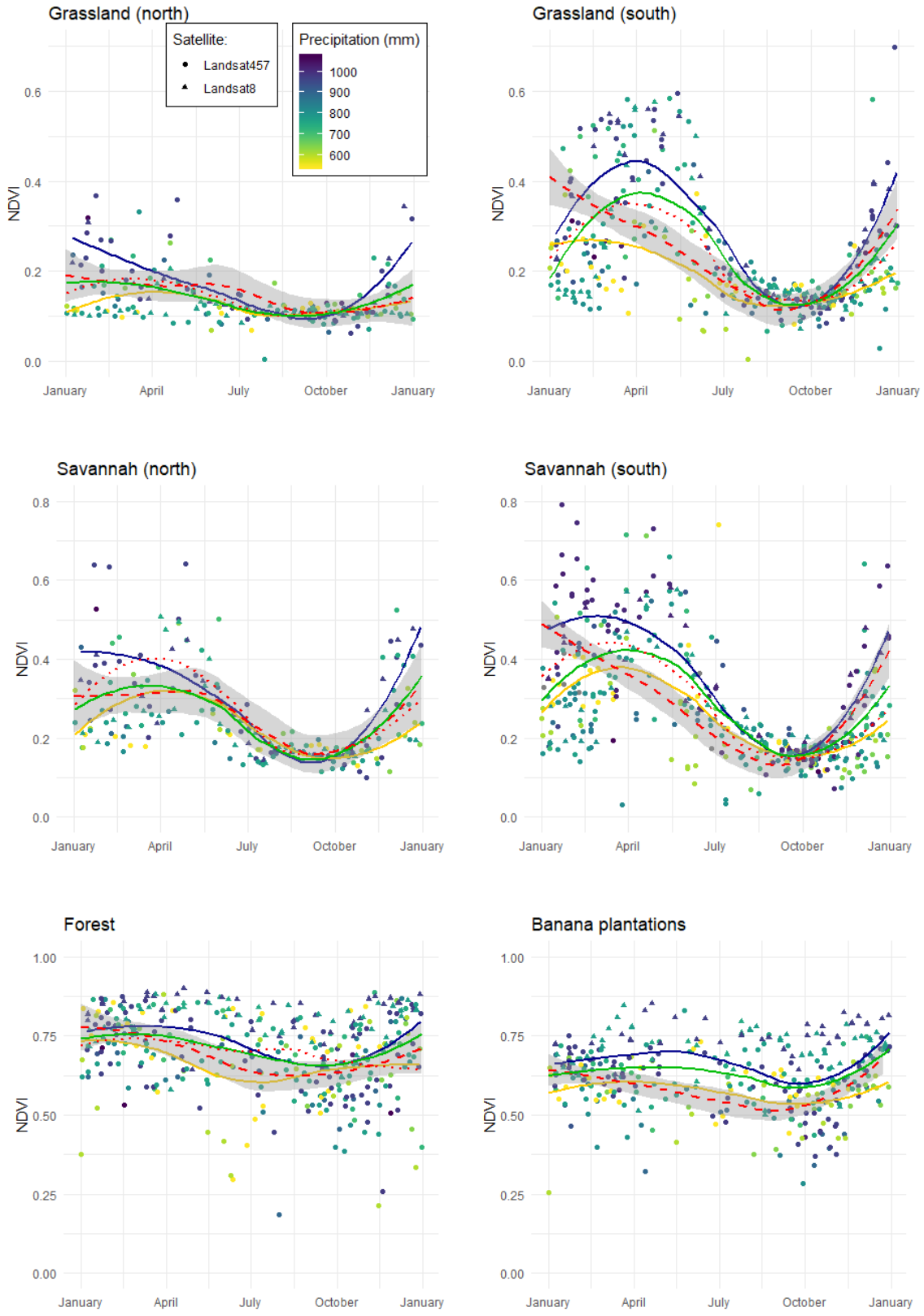
Grassland (north)
Satellite:
Landsat457
Landsat8
Precipitation (mm)
1000
900
800
700
600
NDVI
0.0
0.2
0.4
0.6
January
April
July
October
January
Grassland (south)
Savannah (north)
Savannah (south)
Forest
Banana plantations
0.00
0.25
0.50
0.75
1.00
0.8

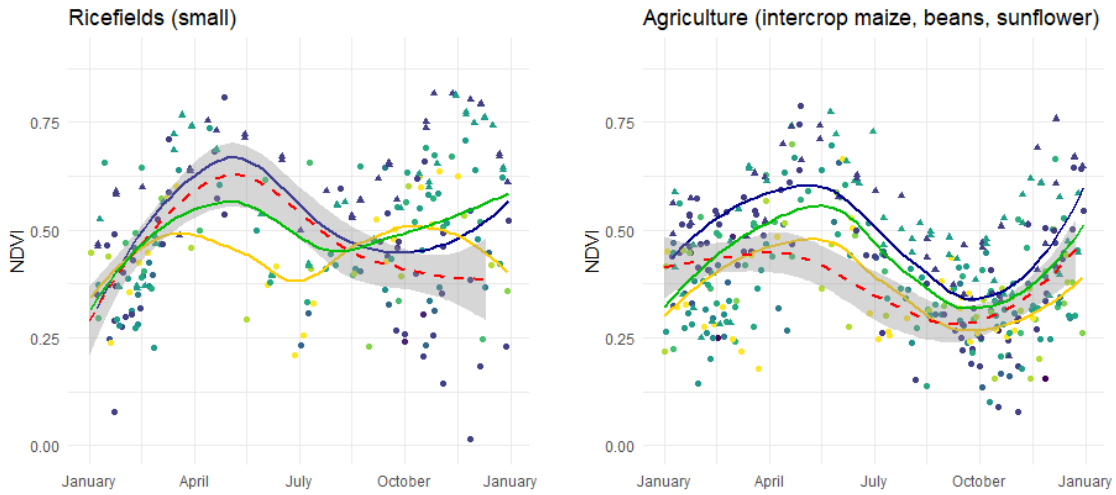

Figure 12: Intra-annual NDVI trends.
Blue = high precipitation; green = average precipitation; yellow = low precipitation; red (dashed) with shadow = NDVI 1 year after a low precipitation year plus one standard deviation; red (dotted) = NDVI 2 years after a low precipitation year.

fields also showed a correlated increase of the NDVI during the dry season. The other areas did not have any significant positive or negative trend.

Table 6: Significant positive trends of long term NDVI (1985-2019) measured over eight different areas during different seasons (wet, dry, annual).

Area	Season	Var(Score)	Denominator	Score	tau	2 sided p-value
Forest	Wet	1833.3	300	118	0.393	0.006
Rice	Wet	1625.3	276	114	0.413	0.005
Banana	Wet	1625.3	276	136	0.493	0.001
Intercrop	Wet	1833.3	300	128	0.427	0.003
Banana	Dry	1257.7	231	143	0.619	6.22E-05
Forest	Annual	3141.7	435	167	0.384	0.003
Rice	Annual	2842.0	406	218	0.537	4.7E-05
Banana	Annual	2842.0	406	196	0.483	0.000
Intercrop	Annual	2842.0	406	170	0.419	0.002

3.3 Perspectives of local people

The people interviewed were living dispersed over an area of 100km^2, belonged to three different villages and two tribes. The majority were Maasai, with only one household being Waarusha. All of the interviewees were agro-pastoralists, although the extend of their agricultural area depended per season on the expectations on rainfall and financial possibilities. One household was also involved in a business of sandal making and distribution. The age of the respondents was between 20 and 103 years old and the time living in the research area differed from ten to over sixty years.

The weather patterns and climate has changed according to the majority. All people mentioning the temperature (6) noticed an increase of temperatures, with some of them noting an increase of extreme heat. The amount of rainfall increased according to two households while the majority of 10 said the precipitation became less with some of

them also mentioning a distortion in the seasonality (3). Multiple households mentioned the drought in 2009, which is also reflected by the meteorological data (TMA, 2019) and indicated a worsening of the both the amount of precipitation and the seasonality.

The availability or quality of grass, an important resource for the livestock of the agro-pastoralists, was decreasing according to all respondents mentioning it (11). Most of them thought this was caused by an increase of livestock (7), but a increase of trees (5), and the decrease of rainfall (4) and fire (1) were also mentioned. The increase of trees in the area was supported by other respondents too (11 in total) but not always linked to the decrease of grassland.

The increase of livestock has led to an increase of competition for grass and other resources. The availability of water increased due to the building of many small dams catching water during the wet season, reducing the competition for water which would have been the main competitive resource. However the increase of the population in the area has led to an increase of cattle, sheep and goats too, resulting in an increase of pressure on the grasslands. Some of the interviewees would seasonally migrate to another location to overcome the effects of diminishing food resources, but this is less favourable nowadays due to the application of agriculture and better accessibility of other services such as education and public transport at their current location.

4 Discussion

4.1 LULC change

This study shows the difficulty of LULC classification in semi-arid regions. The used methods for determining the long term LULC (1985-2019) have not been able to deliver reliable, consistent LULC maps and area sizes over time. Although the tested accuracies on the classified training images resulted in high levels, two factors showed that the outcome does not agree with field observations and visual interpretation of satellite imagery.

LULC class size variability

The first indicator of incorrect classification is the high variability in LULC class area size between the classified maps which were expected not to deviate a lot within a year or a relative short period due to the time it normally takes for a system to change from one class to another. The classes forest, water, and savannah were expected to have very little seasonal changes (Hu and Zhang, 2013). Nonetheless the classes forest and savannah can fluctuate thousands of km^2 within a year (Table B.2). Extreme rainfall events and associated floods could be detected as an (extreme) increase in area of water, and the degradation of land due to (extreme) droughts could be reflected by an increase of bare soil area (especially from grasslands), but this is not expected to this extend.

Table 7: LULC change in semi-arid regions

	Vegetation class	Change over time	Absolute change (km^2)	Change of total area
This research	Bare soil	-73%	4030	27%
	Savannah	54%	2533	17%
Bergh (2016)	Grassland	-55%	916	6%
	Bare soil	57%	1801	11%
Mtui et al. (2017)	Closed shrubland	-28%	173.6	7%
	Woody savannah	-55%	271.1	10%
	Swamp	105%	256.9	10%
John et al. (2009)	Shrubland	-48%	121466	11%
	Bare soil	124%	150790	13%

Many other studies have indicated a LULC change in semi-arid landscapes, but like this study there are big variations in class area size despite the unlikeliness of big changes in woody vegetation (Table 7) (Bergh, 2016; Kiunsi and Meadows, 2006; Mtui et al., 2017; John et al., 2009; Zewdie and Csaplovies, 2015). In these studies less data were used to determine the LULC change (2-4 images versus 32). To overcome possible fluctuations in the classification due to seasonality these studies used images from the same season. As can be seen in Figure 9 this is still ambiguous. The result of this study can demonstrate that with the use of a small amount of images the outcome and conclusions could be reversed if another set of images was used. For example:

- If image 2 and 24 are being compared (respectively Feb 1985 and Jan 2018), in increase in grassland is detected (1137 to 3535 km^2). If image 1 and 29 were used (both Jan, 1987 and 2017) a decrease would have been the result (1978 to 1036 km^2).
- The same applies for respectively a decrease and increase of savannah between the images 2 and 20, or 5 and 25 (6532 to 5943 km^2 (1985-2017); or 8414 to 5943 km^2 (1993-2016)).

Therefore the results of this and other studies, which all have big changes in the LULC classification, are doubtful on the validity of the results (Bergh, 2016; Kiunsi and Meadows, 2006; Mtui et al., 2017; John et al., 2009). The results from Zewdie and Csaplovies (2015), which uses of four images and a smaller amount of classes, show a more realistic, gradual increase of cropland at the expense of forest.

Spectral variations

The second indicator of the incorrect classifications can be found by looking at the individual classified maps. By comparing the original satellite imagery and the result of the classified maps it is visible that errors have been made in the classification. The big changes resulting from the adjusted training dataset indicates that the specific spectral range of each class are close to each other. A small change in either the classifier or the pixel value will therefore result in a different classification map.

Classifier

The change of the classifier, with the use of different ground truth datasets (Table 2), resulted in different LULC class area sizes (Table B.2, Figure 8/10) and classification maps (Figure 11 and D.1-D.6). Despite the lack of a true probability sampling design and therefore a possible bias in the dataset (Stehman and Foody, 2019), the accuracy of the training was high (Table 4). The confusion matrix and associated user's, producer's, and overall accuracies have been mentioned to be the core elements of the accuracy assessment of mapping land cover (Stehman and Foody, 2019). Many other studies obtained an overall accuracy between 0.70 and 0.96 with Kappa ranging between 0.67 to 0.95 which was considered a successful classification and mapping of the study area (Kharazmi et al., 2018). Therefore the accuracies from this research were considered good, but might have been affected by a bias in the sampling data.

Pixel value

It is assumed that the individual pixel value and the spectral range of each class have a bigger effect on the incorrect outcomes because of the high variation of LULC class areas. Every class has a specific spectral range. A pixel value within that range will be assigned to that class. If pixels change easily from one class to another than the pixel values were already at the edge of the range. This can have two explanations.

Firstly, the spectral differences between the classes are small. If the vegetation of two classes is comparable or only a little different, the reference spectra of the two classes are very similar. The transition between the classes forest and savannah, and between savannah and grassland is rather smooth, due to the similarities of the classes in vegetative composition. The spectral difference between for example a big shrub and a small tree will be rather small, resulting in a possible misclassification.

Secondly, the classifier is a static algorithm. It is based on one image at a time with specific climatic conditions. At any other moment these conditions will be different, and so will be the condition of the vegetation. The dynamics of the vegetation will change the pixel values. The value could change such that it is outside the spectral range of its original class. If that is the case it will be assigned to a different class. Sinha (2012) emphasizes the seasonality of LULC in temperate to subtropical climates due to temperature and rainfall. Seasonal trends of those factors result in different vegetation and management response, leading to different phenologies which could be interpreted different from satellite imagery (Gómez et al., 2016). When the imagery of this study is

filtered for a specific season (JFM or ASON), the class area size is still deviating and not unambiguously increasing or decreasing throughout the seasons.

In this research the seasonality is hardly visible (Figure 9). Any trend might be abruptly broken because of the use of two algorithms. For each season a separate classifier was used to decrease the seasonality effect. Due to the high variation in the wet season no trends are visible here, but during the dry season some trends were noted. The decrease of agricultural land and increase of bare soil is a normal appearance due to the harvesting of the crops and the remaining bare land after this. The decrease of forest and increase of grassland don't seem to naturally exchange area, but savannah could be a good mediator for this. During the dry season acacia forests will become less green and therefore shift to the savannah class, whereas the trees and shrubs in the savannah class also become less dominant and shift to the class grassland.

4.2 Vegetation dynamics

Vegetation can change due to numerous causes. According to Teferi et al. (2015) there are three possibilities of how this change appears: (1) the seasonality of the climate (e.g. temperature and rainfall) has an effect on the phenology of vegetation resulting in a cyclic change of the vegetation; (2) a gradual but monotonic change over a longer period of time exists because of a changing environment such as land degradation or a change in land management; and (3) due to a specific event in time the vegetation changes abruptly such as deforestation, floods, droughts and fires.

Precipitation and temperature

The observed non-uniform downward trend of precipitation during the long rains, in Karatu only, is in agreement with findings over the whole of Tanzania where only a few meteo-stations show a downward trend during the long rain season (MAM) or yearly precipitation (United Republic of Tanzania, 2014; Rowell et al., 2015). The observed precipitation levels, the variation and trend is also in line with previous findings (Pardoe et al., 2018; Rowell et al., 2015; Agrawala et al., 2003). However multiple projections predict an increase in rainfall over almost the entirety of the greater Horn of Africa up to 16.3% in 2100 in the north eastern highlands of Tanzania due to thermodynamic effects (United Republic of Tanzania, 2014; Shongwe et al., 2011).

Temperature

The correlated and significant upward trend of temperature has been observed around the whole region, with a similarly stronger trend of mean minimum temperatures (Agrawala et al., 2003; United Republic of Tanzania, 2014). An increase in temperature causes an increase of the potential evapotranspiration (ET_p). Because water is the limiting factor in semi-arid regions, the increase of ET_p will cause a greater stress on the vegetation. A result of greater stress would be a decrease of NDVI, but this was not observed in this research.

Intra-annual NDVI and climate

The NDVI of the natural and agricultural areas in northern Tanzania are characterized by the strong correlation with seasonal rainfall (Table E.4). This is in agreement with other research showing this characteristic in water limited regions (Moulin et al., 1997). The lower correlation (τ) of the forests and the agricultural areas can be linked to the

higher water availability. The forests are located near rivers or mountains where the water availability is higher compared to the lower lying plains. The agricultural areas are under constant human influence, including the manual application of water and fertilizers, positively affecting the living conditions of the vegetation and making it less dependent on rainfall, and negatively affecting the vegetation by harvesting. The natural areas have invariably a lag of 1 month (NDVI response is one month after precipitation) for the best correlation between the precipitation and the NDVI, whereas the agricultural areas have mixed lags dependent on the planting scheme and crop response. The ricefield is not significantly correlated between precipitation and NDVI due to the high anthropogenic influence on this crop.

The intra-annual variation of the NDVI has been lowest for the forest and bananafields compared to the other areas. This can be explained by the year-round evergreen foliage of these systems, resulting in little to no gaps in the canopy. Research by Fuller and Prince (1996) also showed that the interannual CV can be more than doubled for different forest systems such as wet woodland and acacia woodland, with the annual mean NDVI showing a reversed decreasing trend for decreasing precipitation.

The intra-annual variability of the eight areas have seasonal trends as expected. The strong positive correlation between the NDVI and rainfall can be seen in all of the different vegetation classes (Figure 2 and 12). The correlation between the seasonal NDVI and precipitation can also be seen in the differences in NDVI between dry, normal and wet years. During dry years the NDVI is invariably below normal and during wet years above normal NDVI values. Remarkable is the point at the end of the dry season where the NDVI reaches an equal value in a dry, normal or wet year of the savannah and grassland areas. This indicates the depletion of the natural resources for the vegetation, or an equilibrium position to survive during periods of high stress.

Also after a dry year the NDVI is recovering well. The increase of the NDVI after a dry year indicates the resilience of the system, at which the resources are optimally utilized as soon as the conditions allow. Most of the natural systems show a lower than normal NDVI trend after a dry year, but during the second year no significant differences in the intra-annual variability of the NDVI are distinguished. This points to the resilience of the natural systems and the strong resistance to a year of drought. A longer period of stress, such as drought or increased grazing, could lead to a catastrophic vegetation shift. A positive plant-soil feedback could consequently lead to desertification (Rietkerk, 1998). Due to a lack of data the systems have not been tested for any effects of longer periods of drought.

Long term NDVI and climate

Although the high correlation between seasonal rainfall and NDVI, the minimal downward trend of rainfall in Karatu was not reflected by long term NDVI values over the area. The intra-annual NDVI is stronger correlated to precipitation compared to the interannual NDVI (Richard and Poccard, 1998; Daham et al., 2018) which is reflected in this result.

The significant and positive trend in the NDVI of all the agricultural areas was as expected. This can be attributed to a change in the land management. In the year 2012 an improved irrigation system was established at the village of Mto wa Mbu. This caused an improved and more constant water inflow over the area throughout the year. As a result, crops were grown year-round. The NDVI values of the ricefields (Figure 12) also reflect this change in management by a biannual peak of NDVI, representing two growing and harvesting seasons a year.

In the natural vegetative areas the only long term monotonic trend in NDVI that has been found is an increase of NDVI of the forested areas. An increasing trend is shown

in the long rainy season (FMAM) and in the annual NDVI. The cause of this change is unclear because any change in management is unknown, and it is contradictory with the positive trend in temperature and negative trend in rainfall. Theoretically, a gradual revival of the forest could occur due to a fire in the past or a decrease of collection of wood for personal use, but this has not been observed.

A decrease of the NDVI of savannah and grasslands was expected in the Monduli and Longido districts, but no significant trends were measured. An increasing population in the area (NBS, 2013) likely causes enhanced pressure on the system, an increase of mean temperatures (Figure 4) would lead to increased evapotranspiration, and scattered trends of decreasing rainfall (United Republic of Tanzania, 2014) adds to the likeliness of decreasing NDVI in natural areas of northern Tanzania.

The MK trend test does only measure trends over the whole research time period. Any temporal trends, characterized by a turning point (TP) at which the NDVI trend changes from positive to negative or reverse, could be levelled out over the whole time period. If the data showed a decrease up to 2000 and an similar increase up to 2018 this might have a netto zero effect. By incorporating a TP, (other) trends might have been found for both climatological factors as well as the NDVI itself. Changing land management resulting in a changing NDVI does only start at a given moment and not necessarily over the whole period of time of this research. A greening and browning trend was detected over Kenya and Tanzania with a TP in the 1990's, with a net browning trend over the whole time period (1982-2013) (Wei et al., 2018). The different results could be explained by a different dataset and a different methodology that was used, which incorporated the removal of noises and short-term fluctuations in advance.

4.3 Perspective of local people

The results of interviews show that local inhabitants of the rural savannah zone have noticed that temperatures are increasing and rainfall is declining. Also multiple remarks were made about the drought in 2009. These observation correspond with the evidence of changes recorded by one or multiple meteostations nearby. Therefore the information is regarded as generally reliable. There was a great consensus about the increase of trees among the respondents, however without a distinct reason. This could have been measured by the long term trend of NDVI in the savannah (southern part), but has not been detected. The so called ecological transition might result in different vegetation with similar NDVI values and therefore remains untraceable for satellite observations. Also the increased competition for grass was not represented by a decrease of NDVI from grasslands. If any shortages of water and grass were pressing, the old custom of the Maasai to move to a temporal village, especially during the dry season, is still applied. The resilience of the different land cover classes is strong enough to overcome the increased herbivore feeding and decreased rainfall and will be regenerated the next year. However the Maasai implied that the movement to other areas is not longer always favourable, as they gratefully use public services such as education, health care and public transport.

5 Conclusion

In this study an assessment has been done on the long term LULC changes in the Monduli and Longido districts in northern Tanzania with the use of multi-temporal Landsat imagery. A total of 32 images has been collected from the period 1985 to 2019. After the training of two algorithms with the use of ground truth data all images were classified. Despite the high accuracy which resulted from the accuracy assessments en changes that were applied to the training data no conclusions can be drawn on the LULC changes in the research area. The total area of each class was showing big variations over time, which also questions the results of other researches which used a small set of images (¡5). The big variations are presumably caused by the small spectral differences between the classes, and the big variation of the vegetation by the seasons.

Also the dynamics and the resilience of eight different vegetative areas have been studied. This has been done by using long term rainfall data, and obtained NDVI values of each area. Over the period 1985-2019 satellite imagery from Landsat has been collected and the NDVI was calculated. With this data an assessment was done on the long term trends, as well as intra-annual trend analysis and resilience. By analysing the long term NDVI in the dry and wet season and annual means it is proven that all the different agricultural areas have become greener based on the annual averaged NDVI. Of the five natural systems the forested area has become greener in the wet season and the annual NDVI values. The other natural areas have not shown any positive or negative trends.

The intra-annual trend of the NDVI is strongly, positively correlated with the precipitation. For all eight different areas the NDVI is on average higher during a wet season, and lower during a dry season compared to a normal amount of precipitation during the year.

The resilience of the system, measured by using the NDVI values one year or two years after a dry year, is strong. The agricultural areas experience a strong influence of human interactions. In the first year after a dry year lower to normal NDVI values were measured. For the natural areas during the first year after a dry year lower than normal or lower than dry NDVI trend was measured, but in the second year after a dry year the deviation to normal is no longer to be found. This indicates the strong resilience of the systems. Despite the declining trend in rainfall at one of the meteostations and increasing temperatures, the NDVI of the natural systems is constant over time or is increasing and shows a strong resilience.

The local population has also been able to detect changes in the weather, at which an increasing temperature and unreliable rainfall patterns were frequently heard observations. The Maasai indicate that there is an increase in the amount of trees, what has not been detected by changes in the NDVI. The increase of trees is considered as a negative development, which together with an increasing population and herd sizes would lead to the declining availability of grass. The Maasai have been able to solve this problem like they have been doing for a long period in history, by moving to more prosperous land during the dry season. However, this is less favourable for them as they thankfully use services such as education, health care and public transport.

5.1 Recommendations

Shortcomings were revealed in the LULC classification in semi-arid regions. Although the accuracy of the training was good, the outcomes were not sufficient. By determining the exact causes of the misclassification, valuable information would be obtained in order to perform a better LULC analysis. A better understanding of the limitations of the accuracy assessment is needed.

The vegetation dynamics and resilience of the system has been tested with a small dataset and averaged NDVI values over a bigger area. This showed promising results of the resistance of the system to one year of drought. However with a bigger and randomized dataset of locations a better indication of the resilience of the area can be given.

One of the main drivers of LULC change and vegetation dynamics is precipitation. Precipitation measurements in this research area are inconsistent or absent. This causes difficulties for determining years of drought, and possible seasonality changes. A hydrological model which produces a dataset with monthly precipitation would be valuable to solve these unknowns.

An effect of long term drought in combination with the grazing pressure could lead to a tipping point of vegetation shift and lead to land degradation. At this moment the carrying capacity of the system is unknown. Local inhabitants indicate an increase of competition for grazing lands, and the effects of a long term drought on this development is unknown. By assessing the resilience of this and other semi-arid systems to long term drought an insight can be given on the effects. With that information a possible exceedance of the tipping point caused by grazing can be prevented.

Acknowledgements

Many people have contributed in some way to the completion of this thesis, although not all of them are aware.
My supervisors Geert Sterk an Maarten Zeylmans van Emmichoven have been a great help to me, with giving me the opportunity to travel to Tanzania again, but also to try find the solution to solve the unsatisfying results of LULC change, their feedback and patience.
In the field in Tanzania I have received help from many people, but most of all Gift Mayagila. Thanks a lot for all the information, not only about the vegetation and the land, but also about the culture and the nights watching football and watching kids say 'Sivyo mzungu'. But all the people at the agricultural office, Mama Mariam, Mariam, Mailee, Khalid,Dirk, Jill, and many others made me feel comfortable in Mto wa Mbu and Tanzania. And of course Katrijn for all the fun in advance of this journey abroad.

Statement of originality of the MSc thesis

I declare that:

1. this is an original report, which is entirely my work,
2. where I have made use of the ideas of other writers, I have acknowledged the source in all instances,
3. where I have used any diagram or visuals I have acknowledged the source in all instances,
4. this report has not and will not be submitted elsewhere for academic assessment in any other academic course.

Student data:

Name: Steye Laurens Verhoeve

Registration number: 4119274

Date:

August 19, 2019

Signature:

6 References

References

Agrawala, S., Moehner, A., Hemp, A., van Aalst, M., Hitz, S., Smith, J., Meena, H., Mwakifwamba, S. M., Hyera, T., and Mwaipopo, O. U. (2003). Development and climate change in Tanzania: focus on Mount Kilimanjaro. Technical report, Organisation for Economic Co-operation and Development (OECD).

Bergh, H. V. D. (2016). *The impacts of Maasai settlements on land cover, meteorological conditions and wind erosion risk in northern Tanzania*. Master thesis, Utrecht University.

Blake, W. H., Rabinovich, A., Wynants, M., Kelly, C., Nasseri, M., Ngondya, I., Patrick, A., Mtei, K., Munishi, L., Boeckx, P., and Navas, A. (2018). Soil erosion in East Africa: an interdisciplinary approach to realising pastoral land management change. *Environmental Research Letters*, 13(12):124014.

Casalí, J., Giménez, R., and Campo-Bescós, M. (2015). Gully geometry: what are we measuring? *SOIL*, 1(2):509–513.

Chamaille-Jammes, S., Fritz, H., and Murindagomo, F. (2006). Spatial patterns of the NDVI-rainfall relationship at the seasonal and interannual time scales in an African savanna. *International Journal of Remote Sensing*, 27(23):5185–5200.

Cherlet, M., Hutchinson, C., Reynolds, J., Hill, J., Sommer, S., and von Maltitz, G. (2018). *World Atlas of Desertification*. Publication Office of the European Union, Luxembourg, 3rd edition.

Conroy, A. B. (2001). *Maasai oxen, agriculture and land use change in Monduli District, Tanzania*. Doctoral dissertations, University of New Hampshire, Durham.

Daham, A., Han, D., Rico-Ramirez, M., and Marsh, A. (2018). Analysis of NVDI variability in response to precipitation and air temperature in different regions of Iraq, using MODIS vegetation indices. *Environmental Earth Sciences*, 77(10):389.

Decentralized Climate Finance Project (2019). Pilot Districts.

Degen, J. (2015). *Impact of land cover and soil conservation on soil erosion rates in the Tikur Woha Catchment, Ethiopia*. Master thesis, Utrecht University.

Forkel, M., Carvalhais, N., Verbesselt, J., Mahecha, M. D., Neigh, C. S. R., and Reichstein, M. (2013). Trend Change Detection in NDVI Time Series: Effects of Inter-Annual Variability and Methodology. *Remote Sensing*, 5(5):2113–2144.

Fratkin, E. (2001). East African Pastoralism in Transition: Maasai, Boran, and Rendille Cases. *African Studies Review*, 44(3):1–25.

Fuller, D. O. and Prince, S. D. (1996). Rainfall and foliar dynamics in tropical Southern Africa: Potential impacts of global climatic change on savanna vegetation. *Climatic Change*, 33(1):69–96.

Galvin, K. A., Thornton, P. K., Boone, R. B., and Sunderland, J. (2004). Climate variability and impacts on east African livestock herders: The Maasai of Ngorongoro Conservation Area, Tanzania. *African Journal of Range and Forage Science*, 21(3):183–189.

Gislason, P. O., Benediktsson, J. A., and Sveinsson, J. R. (2006). Random Forests for land cover classification. *Pattern Recognition Letters*, 27(4):294–300.

Gómez, C., White, J. C., and Wulder, M. A. (2016). Optical remotely sensed time series data for land cover classification: A review. *ISPRS Journal of Photogrammetry and Remote Sensing*, 116:55–72.

Google Earth (2013). Gully erosion, 3 25'07.71S, 35 57'37.12E, elevation 1.34 km, date of imagery: 2013-01-23; 2015-01-14; 2017-01-13; 2017-03-13. \url{http://www.google.com/earth/index.html}.

Gorelick, N., Hancher, M., Dixon, M., Ilyushchenko, S., Thau, D., and Moore, R. (2017). Google Earth Engine: Planetary-scale geospatial analysis for everyone. *Remote Sensing of Environment*, 202:18–27.

Hammond Murray-Rust, D. (1972). Soil Erosion and Reservoir Sedimentation in a Grazing Area West of Arusha , Northern Tanzania. *Geografiska Annaler*, 54(9):325–343.

Homewood, K., Kristjanson, P., and Chenevix Trench, P. (2009). Changing Land Use, Livelihoods and Wildlife Conservation in Maasailand. In Homewood, K., Kristjanson, P., and Chenevix Trench, P., editors, *Staying Maasai? Livelihoods, Conservation and Development in East African Rangelands*, chapter 1, pages 1–42. Springer Press, London.

Hu, J. and Zhang, Y. (2013). Seasonal change of land-use/land-cover (LULC) detection using modis data in rapid urbanization regions: A case study of the Pearl River delta region (China). *IEEE Journal of Selected Topics in Applied Earth Observations and Remote Sensing*, 6(4):1913–1920.

Interim Secretariat (1994). International Convention to Combat Desertification in Countries. Technical report, United Nations, New York.

Ionita, I., Fullen, M. A., Zgłobicki, W., and Poesen, J. (2015). Gully erosion as a natural and human-induced hazard. *Natural Hazards*, 79(1):1–5.

Iqbal, M. F. and Khan, I. A. (2014). Spatiotemporal Land Use Land Cover change analysis and erosion risk mapping of Azad Jammu and Kashmir, Pakistan. *Egyptian Journal of Remote Sensing and Space Science*, 17(2):209–229.

John, R., Chen, J., Lu, N., and Wilske, B. (2009). Land cover/land use change in semi-arid Inner Mongolia: 19922004. *Environmental Research Letters*, 4(4):45010.

Ju, J. and Masek, J. G. (2016). The vegetation greenness trend in Canada and US Alaska from 1984–2012 Landsat data. *Remote Sensing of Environment*, 176:1 – 16.

Kharazmi, R., Tavili, A., Rahdari, M. R., Chaban, L., Panidi, E., and Rodrigo-Comino, J. (2018). Monitoring and assessment of seasonal land cover changes using remote sensing: a 30-year (1987–2016) case study of Hamoun Wetland, Iran. *Environmental Monitoring and Assessment*, 190(6):356.

Kiunsi, R. B. and Meadows, M. E. (2006). Assessing land degradation in the Monduli District, northern Tanzania. *Land Degradation and Development*, 17(5):509–525.

Lanorte, A., Manzi, T., Nolè, G., and Lasaponara, R. (2015). On the Use of the Principal Component Analysis (PCA) for Evaluating Vegetation Anomalies from LANDSAT-TM NDVI Temporal Series in the Basilicata Region (Italy) BT. In Gervasi, O., Murgante, B., Misra, S., Gavrilova, M. L., Rocha, A. M. A. C., Torre, C., Taniar, D., and Apduhan, B. O., editors, *Computational Science and Its Applications – ICCSA 2015*, pages 204–216, Cham. Springer International Publishing.

Loveland, T. R. and Belward, A. S. (1997). The IGBP-DIS global 1km land cover data set, DISCover: First results. *International Journal of Remote Sensing*, 18(15):3289–3295.

Maerker, M., Quénéhervé, G., Bachofer, F., and Mori, S. (2015). A simple DEM assessment procedure for gully system analysis in the Lake Manyara area, northern Tanzania. *Natural Hazards*, 79:235–253.

Mbatha, N. and Xulu, S. (2018). Time Series Analysis of MODIS-Derived NDVI for the Hluhluwe-Imfolozi Park, South Africa: Impact of Recent Intense Drought. *Climate*, 6(4).

Middleton, N. and Thomas, D. (1997). *World Atlas of Desertification*. United Nations Environment Program, New York, 2 edition.

Midekisa, A., Holl, F., Savory, D. J., Andrade-Pacheco, R., Gething, P. W., Bennett, A., and Sturrock, H. J. (2017). Mapping land cover change over continental Africa using Landsat and Google Earth Engine cloud computing. *PLoS ONE*, 12(9):1–15.

Millard, K. and Richardson, M. (2015). On the Importance of Training Data Sample Selection in Random Forest Image Classification: A Case Study in Peatland Ecosystem Mapping. *Remote Sensing*, 7:8489–8515.

Millenium Ecosystem Assessment (2005). Ecosystems and Human Well-Being, synthesis. Technical report, Millennium Ecosystem Assessment, Washington DC.

Moulin, S., Kergoat, L., Viovy, N., and Dedieu, G. (1997). Global-Scale Assessment of Vegetation Phenology Using NOAA/AVHRR Satellite Measurements. *Journal of Climate*, 10(6):1154–1170.

Msoffe, F. U., Kifugo, S. C., Said, M. Y., Neselle, M. O., Van Gardingen, P., Reid, R. S., Ogutu, J. O., Herero, M., and de Leeuw, J. (2011). Drivers and impacts of land-use change in the Maasai Steppe of northern Tanzania: an ecological, social and political analysis. *Journal of Land Use Science*, 6(4):261–281.

Mtui, D. T., Lepczyk, C. A., Chen, Q., Miura, T., and Cox, L. J. (2017). Assessing multi-decadal land-cover - land-use change in two wildlife protected areas in Tanzania using Landsat imagery. *PLoS ONE*, 12(9):1–20.

Mwalyosi, R. B. (1992). Land-use Changes and Resource Degradation in South–West Masailand, Tanzania. *Environmental Conservation*, 19(02):145.

Nasanbat, E., Sharav, S., Sanjaa, T., Lkhamjav, O., Magsar, E., and Tuvdendorj, B. (2018). Frequency analysis of MODIS NDVI time series for determining hotspot of land degradation in Mongolia. *Int. Arch. Photogramm. Remote Sens. Spatial Inf. Sci.*, XLII-3:1299–1304.

NBS (2013). 2012 Population and Housing Census. Technical report, National Bureau of Statistics (NBS), Dar es Salaam.

NBS (2017). National Environment Statistics Report (NESR,2017) - Tanzania Mainland. Technical report, National Bureau of Statistics (NBS), Dar es Salaam.

Pardoe, J., Conway, D., Namaganda, E., Vincent, K., Dougill, A. J., and Kashaigili, J. J. (2018). Climate change and the water–energy–food nexus: insights from policy and practice in Tanzania. *Climate Policy*, 18(7):863–877.

Prins, H. (1987). Nature conservation as an integral part of optimal land use in East Africa: The case of the Masai ecosystem of Northern Tanzania. *Biological Conservation*, 40(2):141–161.

Pullanikkatil, D., Palamuleni, L. G., and Ruhiiga, T. M. (2016). Land use/land cover change and implications for ecosystems services in the Likangala River Catchment, Malawi. *Physics and Chemistry of the Earth*, 93:96–103.

Quénéhervé, G., Bachofer, F., and Maerker, M. (2015). Experimental assessment of runoff generation processes on hillslope scale in a semiarid region in Northern Tanzania. *Geografia Fisica e Dinamica Quaternaria*, 38(1):55–66.

Richard, Y. and Poccard, I. (1998). A statistical study of NDVI sensitivity to seasonal and interannual rainfall variations in Southern Africa. *International Journal of Remote Sensing*, 19(15):2907–2920.

Rietkerk, M. (1998). *Catastrophic vegetation dynamics and soil degradation in semi-arid grazing systems*. PhD thesis, Wageningen University of Research.

Rossiter, D. (2014). Technical Note: Statistical methods for accuracy assesment of classified thematic maps.

Rowell, D. P., Booth, B. B. B., Nicholson, S. E., and Good, P. (2015). Reconciling Past and Future Rainfall Trends over East Africa. *Journal of Climate*, 28(24):9768–9788.

Roy, D. P., Kovalskyy, V., Zhang, H. K., Vermote, E. F., Yan, L., Kumar, S. S., and Egorov, A. (2016). Characterization of Landsat-7 to Landsat-8 reflective wavelength and normalized difference vegetation index continuity. *Remote Sensing of Environment*, 185:57–70.

She, X., Zhang, L., Cen, Y., Wu, T., Huang, C., and Baig, M. H. A. (2015). Comparison of the Continuity of Vegetation Indices Derived from Landsat 8 OLI and Landsat 7 ETM+ Data among Different Vegetation Types. *Remote Sensing*, 7(10):13485–13506.

Shongwe, M. E., van Oldenborgh, G. J., van den Hurk, B., and van Aalst, M. (2011). Projected Changes in Mean and Extreme Precipitation in Africa under Global Warming. Part II: East Africa. *Journal of Climate*, 24(14):3718–3733.

Sinha, P. (2012). Three-date landsat thematic mapper composite in seasonal land-cover change identification in a mid-latitudinal region of diverse climate and land use. *Journal of Applied Remote Sensing*, 6:63591–63595.

Stehman, S. V. and Foody, G. M. (2019). Key issues in rigorous accuracy assessment of land cover products. *Remote Sensing of Environment*, 231:111199.

Steven, M. D., Malthus, T. J., Baret, F., Xu, H., and Chopping, M. J. (2003). Intercalibration of vegetation indices from different sensor systems. *Remote Sensing of Environment*, 88(4):412 – 422.

Tal, A. and Cohen, J. A. (2007). Bringing Top-down to Bottom-up: A New Role for Environemtal Legislation in Combating Desertification. *Harvard Environmental Law Review*, 31(1):163–271.

Tangud, T., Nasahara, K., Borjigin, H., and Bagan, H. (2018). Land-cover change in the Wulagai grassland, Inner Mongolia of China between 1986 and 2014 analysed using multi-temporal Landsat images. *Geocarto International*, 6049(May):1–15.

Teferi, E., Uhlenbrook, S., and Bewket, W. (2015). Inter-annual and seasonal trends of vegetation condition in the Upper Blue Nile (Abay) Basin: Dual-scale time series analysis. *Earth System Dynamics*, 6(2):617–636.

TMA (2019). Daily rainfall data, monthly rainfall data, monthly temperature data. Retrieved through personal communication. Technical report, Tanzanian Meteorological Agency.

UN OCHA ROSA (2018). Tanzania administrative level 0 - 3 boundaries.

United Republic of Tanzania (2014). Second National Communication to the United Nations Framework Convention on Climate Change. Technical report, Division of Environment, Vice President's Office, Dar es Salaam.

Wei, F., Wang, S., Fu, B., Pan, N., Feng, X., Zhao, W., and Wang, C. (2018). Vegetation dynamic trends and the main drivers detected using the ensemble empirical mode decomposition method in East Africa. *Land Degradation and Development*, 29(8):2542–2553.

Wickama, J., Okoba, B., and Sterk, G. (2014). Effectiveness of sustainable land management measures in West Usambara highlands, Tanzania. *Catena*, 118:91–102.

WISP (2008). Policies that work for pastoral environments. Technical report, The World Initiative for Sustainable Pastoralism (WISP), Nairobi.

Xie, Z., Huete, A., Ma, X., Restrepo-coupe, N., Devadas, R., Clarke, K., and Lewis, M. (2016). Landsat and GRACE observations of arid wetland dynamics in a dryland river system under multi-decadal hydroclimatic extremes. *Journal of Hydrology*, 543:818–831.

Xiong, J., Thenkabail, P. S., Tilton, J. C., Gumma, M. K., Teluguntla, P., Id, A. O., Id, R. G. C., Id, K. Y., and Gorelick, N. (2016). Nominal 30-m Cropland Extent Map of Continental Africa by Integrating Pixel-Based and Object-Based Algorithms Using Sentinel-2 and Landsat-8 Data on Google Earth Engine. *Remote Sensing*, 9(1065):1–27.

Zewdie, W. and Csaplovies, E. (2015). Remote Sensing based multi-temporal land cover classification and change detection in northwestern Ethiopia. *European Journal of Remote Sensing*, 48(1):121–139.

Zhu, Z., Wang, S., and Woodcock, C. E. (2015). Improvement and expansion of the Fmask algorithm: cloud, cloud shadow, and snow detection for Landsats 4–7, 8, and Sentinel 2 images. *Remote Sensing of Environment*, 159:269–277.

Appendices

Appendix A Sensor bands

Table A.1: Properties of the Landsat TM and Landsat EMT+ sensors

	Landsat 4/5 (TM)				Landsat 7 (ETM+)			
Band description	Band name	Spatial resolution (m)	Spectral Wavelengths (µm) Min	Max	Band name	Spatial resolution (m)	Spectral Wavelengths (µm) Min	Max
Blue	B1	30	0.45	0.52	B1	30	0.45	0.515
Green	B2	30	0.52	0.6	B2	30	0.525	0.605
Red	B3	30	0.63	0.69	B3	30	0.63	0.69
NIR	B4	30	0.76	0.9	B4	30	0.775	0.9
SWIR1	B5	30	1.55	1.75	B5	30	1.55	1.75
SWIR2	B7	30	2.08	2.35	B7	30	2.09	2.35
TIR1	B6	120	10.4	12.5	B6_VCID	60	10.4	12.5
Panchromatic	-	-	-	-	B8	13x15	0.52	0.9

Table A.2: Properties of the Landsat OLI-TIRS and Sentinel MSI sensors

	Landsat 8 OLI-TIRS				Sentinel 2A/2B MSI			
Band description	Band name	Spatial resolution (m)	Spectral Wavelengths (µm) Min	Max	Band name	Spatial resolution (m)	Spectral Wavelengths (µm) Min	Max
Aerosol	B1	30	0.435	0.451	B1	60	0.433	0.453
Blue	B2	30	0.452	0.512	B2	10	0.4575	0.5225
Green	B3	30	0.533	0.59	B3	10	0.5425	0.5775
Red	B4	30	0.636	0.673	B4	10	0.65	0.68
Red Edge 1	-	-	-	-	B5	20	0.6975	0.7125
Red Edge 2	-	-	-	-	B6	20	0.7325	0.7475
Red Edge 3	-	-	-	-	B7	20	0.773	0.793
NIR	B5	30	0.851	0.879	B8	10	0.7845	0.8995
Red Edge 4	-	-	-	-	B8a	20	0.855	0.875
Panchromatic	B8	15	0.503	0.676	-	-	-	-
Water Vapour	-	-	-	-	B9	60	0.935	0.955
Cirrus	B9	30	1.363	1.384	B10	60	1.36	1.39
SWIR1	B6	30	1.566	1.651	B11	20	1.565	1.655
SWIR2	B7	30	2.107	2.294	B12	20	2.1	2.28
TIR1	B10	100	10.6	11.19	-	-	-	-
TIR2	B11	100	11.5	12.51	-	-	-	-

Appendix B LULC images

Table B.1: Imagery used for the training of the classifier. Dark gray are images acquired during the wet season, light gray are images acquired during the dry season.

Acquisition date	Satellite and sensor	Cloud cover	WRS path	WRS row
9-Sep-2018		0	169	62
18-Sep-2018		7	168	62
18-Sep-2018	Landsat 7 ETM+	2	168	63
31-Jan-2019		0	169	62
24-Jan-2019		3	168	62
24-Jan-2019		9	168	63
3-Dec-2017		6.83	169	62
23-Sep-2017		0	168	63
23-Sep-2017	Landsat 8 OLI-TIRS	1.58	168	62
12-Mar-2019		0.17	169	62
21-Mar-2019		1.43	168	62
21-Mar-2019		4.71	168	63

Table B.2: The total area of each LULC class in km^2 with dataset 6. Images used for classification. Cloud cover is relative over the study area (%). Dark gray are images acquired during the wet season, light gray are images acquired during the dry season.

#	Date	Satellite and sensor	Cloud cover	Forest	Savannah	Grassland	Cropland	Bare	Water
1	18-Jan-1985	L5 TM	3.31	326	5608	1978	852	5456	19
2	25-Feb-1987	L5 TM	3.26	335	6532	1137	1217	4953	94
3	1-Oct-1988	L4 TM	0.16	477	8638	1937	221	3539	75
4	17-Oct-1988	L4 TM	0.23	490	8416	2422	205	3199	49
5	17-Feb-1993	L4 TM	4.43	1655	8414	882	1531	2096	73
6	30-Jan-1995	L5 TM	6.13	347	5247	943	1053	5680	17
7	4-Nov-2009	L5 TM	0.39	615	7153	2031	279	4639	183
8	8-Jun-2013	L8 OLI-TIRS	7.19	1635	7749	1502	2329	607	488
9	27-Aug-2013	L8 OLI-TIRS	2.91	1064	8604	1911	1346	1157	361
10	28-Sep-2013	L8 OLI-TIRS	4.2	802	9072	1387	1250	1402	250
11	30-Oct-2013	L8 OLI-TIRS	5.39	591	7613	2415	1041	1616	374
12	15-Nov-2013	L8 OLI-TIRS	1.23	1004	7839	2001	2012	1401	382
13	3-Feb-2014	L8 OLI-TIRS	0.89	1033	8862	1773	2012	978	153
14	13-Jul-2014	L8 OLI-TIRS	4.29	1839	8137	1116	1624	1613	282
15	15-Sep-2014	L8 OLI-TIRS	7.26	655	6710	1591	1394	1612	320
16	20-Dec-2014	L8 OLI-TIRS	5.51	1479	7756	1007	2666	670	409
17	10-Mar-2015	L8 OLI-TIRS	1.21	671	8206	2235	1878	1424	202
18	18-Sep-2015	L8 OLI-TIRS	8.96	461	7328	2215	1140	1510	219
19	8-Jan-2016	L8 OLI-TIRS	4.51	2001	7906	1093	2471	566	223
20	25-Feb-2016	L8 OLI-TIRS	9.9	2032	5943	1099	2991	452	638
21	28-Mar-2016	L8 OLI-TIRS	1.7	1115	8871	1517	2035	992	163
22	3-Aug-2016	L8 OLI-TIRS	1.08	1696	8591	1153	1787	1252	253
23	22-Oct-2016	L8 OLI-TIRS	0.9	557	8803	2451	942	1770	199
24	26-Jan-2017	L8 OLI-TIRS	1.53	394	6476	3535	1783	2149	213
25	11-Feb-2017	L8 OLI-TIRS	1.87	497	7236	2734	1779	2004	151
26	23-Sep-2017	L8 OLI-TIRS	0.02	513	8468	2147	2013	1497	189
27	12-Dec-2017	L8 OLI-TIRS	9.21	485	6053	2420	1786	1915	565
28	28-Dec-2017	L8 OLI-TIRS	3.91	253	7424	2538	1445	2904	103
29	29-Jan-2018	L8 OLI-TIRS	1.76	1545	8415	1036	2619	725	189
30	12-Oct-2018	L8 OLI-TIRS	8.58	860	8201	1911	586	1565	411
31	1-Feb-2019	L8 OLI-TIRS	6.96	1297	7268	1492	2228	802	462
32	21-Mar-2019	L8 OLI-TIRS	1.48	497	8141	2652	1534	1426	216

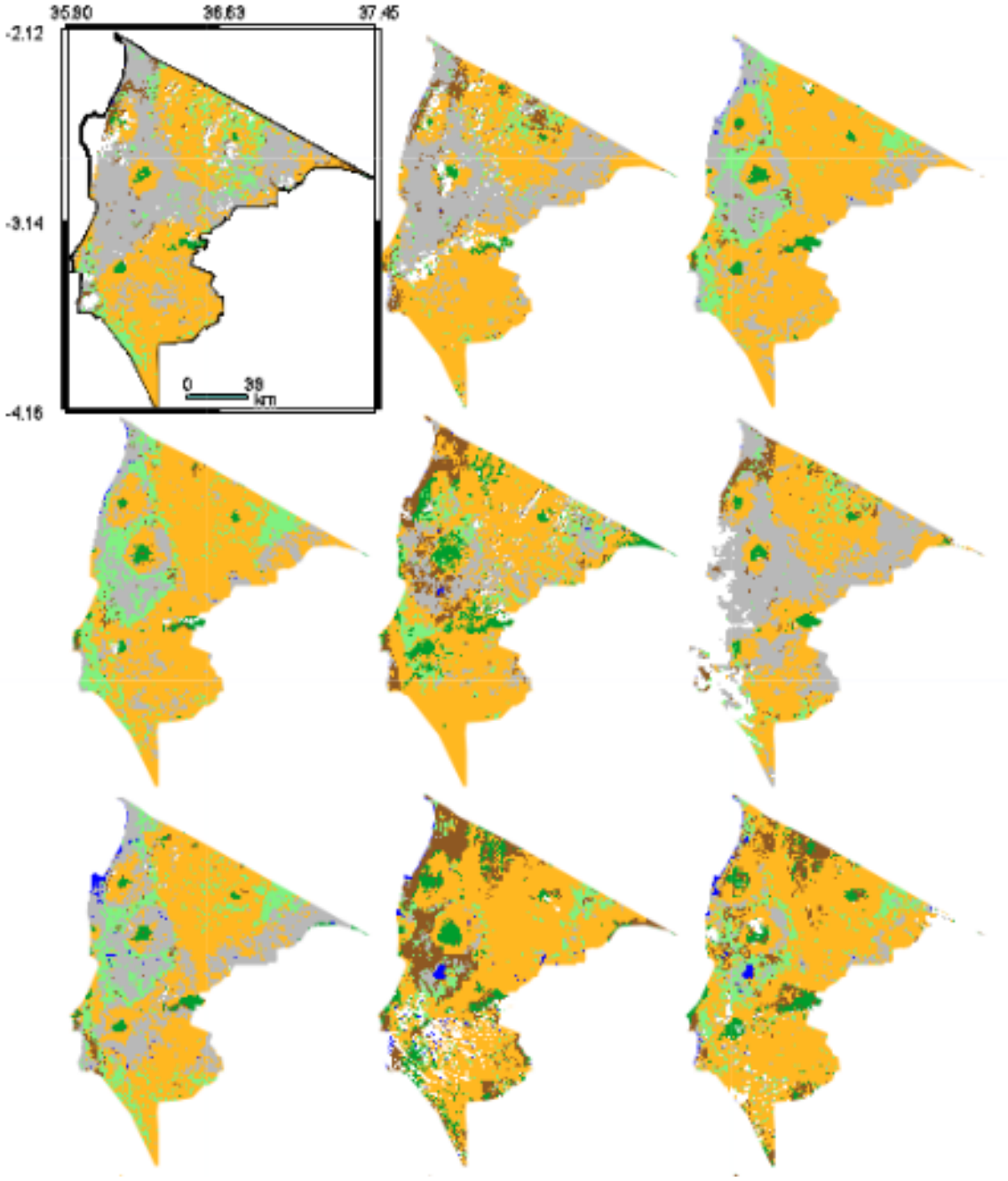

Figure B.1: Land cover maps from 18 Jan 1985 to 27 Aug 2013

Figure B.2: Land cover maps from 28 Sep 2013 to 18 Sep 2015

Figure B.3: Land cover maps from 8 Jan 2016 to 12 Dec 2017

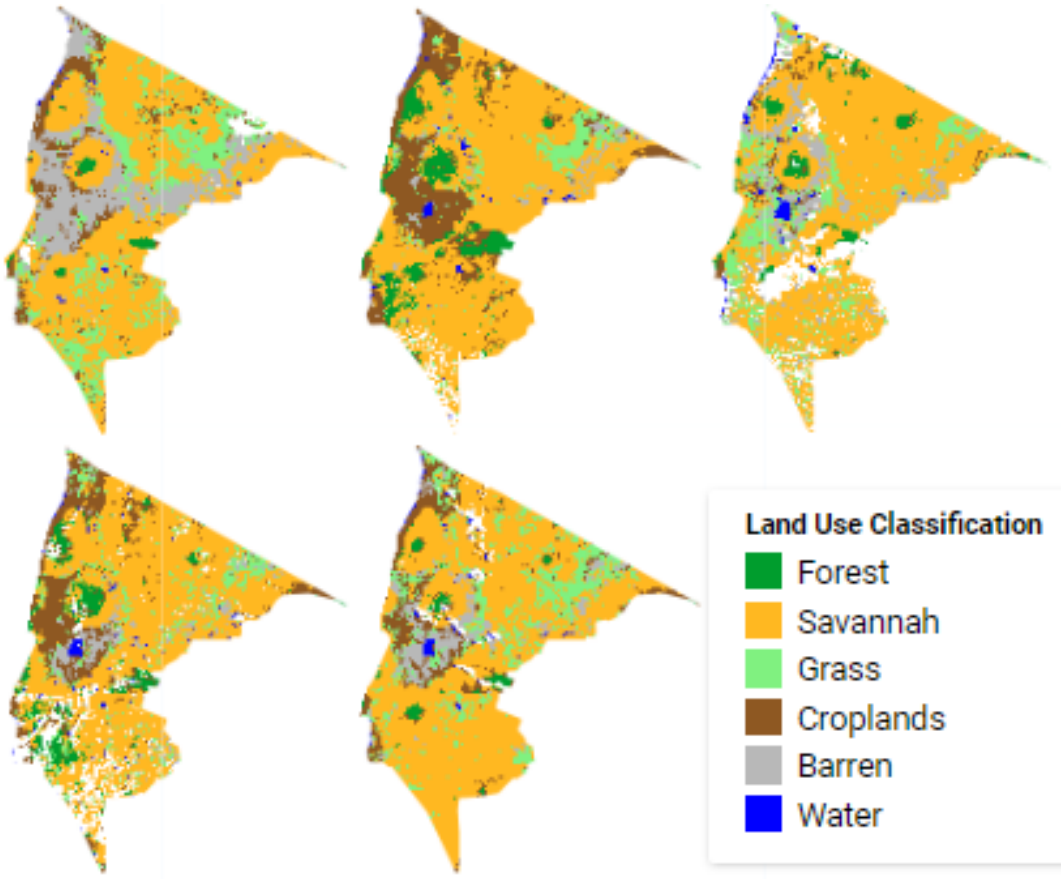

Figure B.4: Land cover maps from 28 Dec 2017 to 21 Mar 2019 and a legend.
Source: https://code.earthengine.google.com/d26ccffb653761aeaf177475195d7eae

Appendix C Confusion matrix

Abbreviations:

Sav. = Savannah
Agr. = Agriculture
Inc. class. = Incorrect classified
Err. of Com. = Error of Commission
User's acc. = User's accuracy
Error of Om = Error of Omission
Prod. Acc. = Producers Accuracy

Confusion matrixes from the training with dataset 5

Table C.1: Confusion matrix of the training of the classifier with dataset 5 on Landsat 7 imagery.

	Forest (moist)	Forest (dry)	Sav.	Grass	Agr.	Bare	Water	Total	Inc. class.	Err. of com.	User's acc.
Forest (moist)	3304	0	0	0	1	0	0	3305	1	0	1
Forest (dry)	1	8	0	0	1	0	0	10	2	0.200	0.800
Savannah	0	0	81	0	3	1	0	85	4	0.047	0.953
Grass	0	0	8	77	0	0	0	85	8	0.094	0.906
Agriculture	0	0	1	0	62	0	0	63	1	0.016	0.984
Bare	0	0	2	0	0	17	0	19	2	0.105	0.895
Water	0	0	2	0	0	0	209	211	2	0.009	0.991
Total	3305	8	94	77	67	18	209	3778			
Inc. class.	1	0	13	0	5	1	0				
Error of om.	0.000	0	0.138	0	0.075	0.056	0				
Prod. Acc.	1.000	1	0.862	1	0.925	0.944	1	0.995			

Table C.2: Confusion matrix of the training of the classifier with dataset 5 on Landsat 8 imagery.

	Forest (moist)	Forest (dry)	Sav.	Grass	Agr.	Bare	Water	Total	Inc. class.	Err. of com.	User's acc.
Forest (moist)	4866	0	0	0	1	0	0	4867	1	0	1
Forest (dry)	4	17	0	0	0	0	0	21	4	0.190	0.810
Savannah	1	2	102	7	2	0	0	114	10	0.088	0.895
Grass	0	0	7	105	0	0	0	112	7	0.063	0.938
Agriculture	0	0	0	46	0	0	0	46	46	1	0
Bare	1	0	2	2	0	20	0	25	5	0.200	0.800
Water	0	0	1	2	0	1	218	222	4	0.018	0.982
Total	4872	19	112	162	3	21	218	5407			
Inc. class.	6	2	10	57	3	1	0				
Error of om.	0.001	0.105	0.089	0.352	1	0.048	0				
Prod. Acc.	0.999	0.895	0.911	0.648	0	0.952	1	0.985			

Confusion matrices from the training with dataset 6

Table C.3: Confusion matrix of the training of the classifier with dataset 6 on Landsat 7 imagery of the wet season.

	Forest	Sav.	Grass	Agr.	Bare	Water	Total	Inc. class.	Err. of com.	User's acc.
Forest	154	1	0	0	0	0	155	1	0.006	0.994
Savannah	1	111	2	2	2	0	118	7	0.059	0.941
Grass	0	4	81	0	0	0	85	4	0.047	0.953
Agriculture	0	7	0	86	0	0	93	7	0.075	0.925
Bare	0	3	0	1	23	0	27	4	0.148	0.852
Water	0	0	0	0	0	38	38	0	0	1
Total	155	126	83	89	25	38	516			
Inc. class.	1	15	2	3	2	0				
Error of om.	0.006	0.119	0.024	0.034	0.08	0				
Prod. Acc.	0.994	0.881	0.976	0.966	1	1	0.955			

Table C.4: Confusion matrix of the training of the classifier with dataset 6 on Landsat 7 imagery of the dry season.

	Forest	Sav.	Grass	Agr.	Bare	Water	Total	Inc. class.	Err. of com.	User's acc.
Forest	142	1	0	0	0	0	143	1	0.007	0.993
Savannah	2	125	6	0	0	0	133	8	0.060	0.940
Grass	0	4	78	0	0	0	82	4	0.049	0.951
Agriculture	0	1	1	72	0	0	74	2	0.027	0.973
Bare	0	0	0	0	23	0	23	0	0	1
Water	0	0	0	0	0	55	55	0	0	1
Total	144	131	85	72	23	55	510			
Inc. class.	2	6	7	0	0	0				
Error of om.	0.014	0.046	0.082	0	0	0				
Prod. Acc.	0.986	0.954	0.918	1	1	1	0.971			

Table C.5: Confusion matrix of the training of the classifier with dataset 6 on Landsat 8 imagery of the wet season.

	Forest	Sav.	Grass	Agr.	Bare	Water	Total	Inc. class.	Err. of com.	User's acc.
Forest	190	3	0	2	0	0	195	5	0.026	0.974
Savannah	0	146	3	1	0	0	150	4	0.027	0.973
Grass	0	14	91	0	0	0	105	14	0.133	0.867
Agriculture	0	1	0	71	0	0	72	1	0.014	0.986
Bare	0	1	3	1	25	0	30	5	0.167	0.833
Water	0	2	0	0	0	67	69	2	0.029	0.971
Total	190	167	97	75	25	67	621			
Inc. class.	0	21	6	4	0	0				
Error of om.	0	0.126	0.062	0.053	0	0				
Prod. Acc.	1	0.874	0.938	0.947	1	1	0.950			

Table C.6: Confusion matrix of the training of the classifier with dataset 6 on Landsat 8 imagery of the dry season.

	Forest	Sav.	Grass	Agr.	Bare	Water	Total	Inc. class.	Err. of com.	User's acc.
Forest	179	2	0	1	0	0	182	3	0.016	0.984
Savannah	0	45	4	2	0	0	151	6	0.040	0.960
Grass	0	9	96	0	0	0	105	9	0.086	0.914
Agriculture	0	1	0	116	0	0	117	1	0.009	0.991
Bare	0	0	2	0	22	0	24	2	0.083	0.917
Water	0	0	0	0	0	41	41	0	0	1
Total	179	157	102	119	22	41	620			
Inc. class.	0	12	6	3	0	0				
Error of om.	0	0.076	0.059	0.025	0	0				
Prod. Acc.	1	0.924	0.941	0.975	1	1	0.966			

Appendix D LULC classified maps

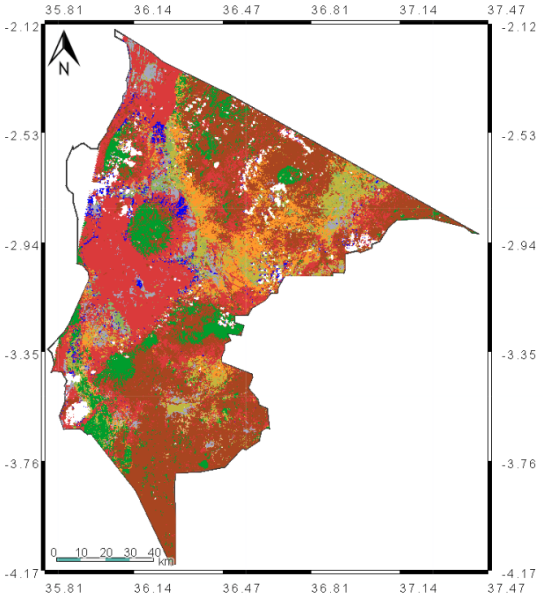

(a) 18 Jan 1985 (wet season)

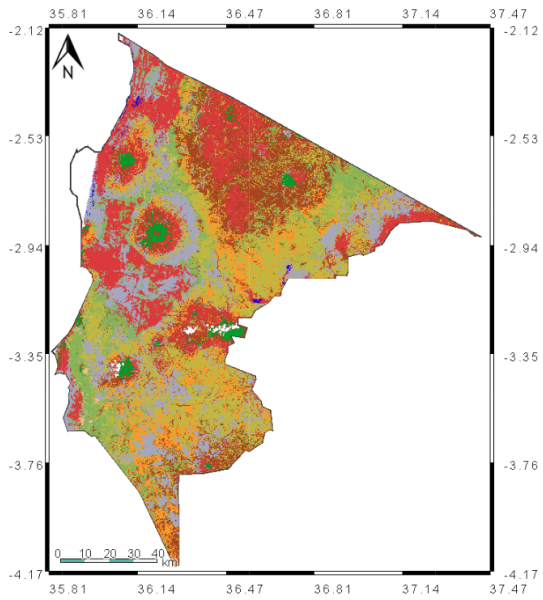

(b) 17 Oct 1988 (dry season)

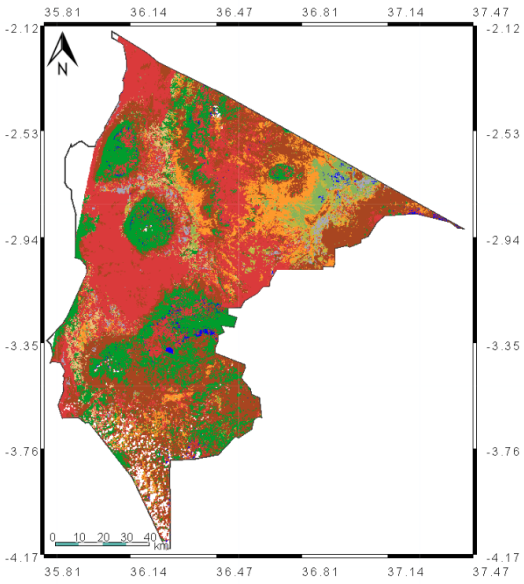

(c) 29 Jan 2018 (wet season)

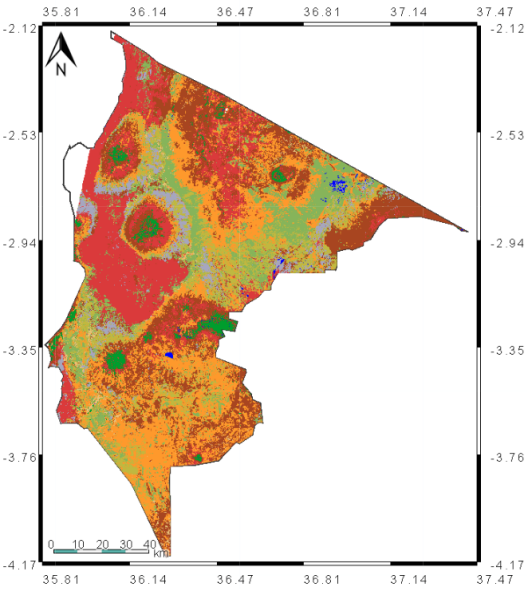

(d) 23 Sep 2017 (dry season)

(e) Legend

Figure D.1: Land cover maps based on dataset 1, ungrouped classes.
Source: https://code.earthengine.google.com/d88e11f0b078168de6da82310fc7d2bd

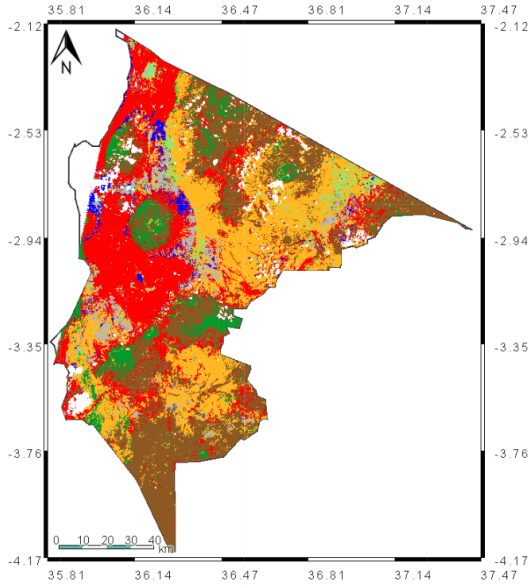

(a) 18 Jan 1985 (wet season)

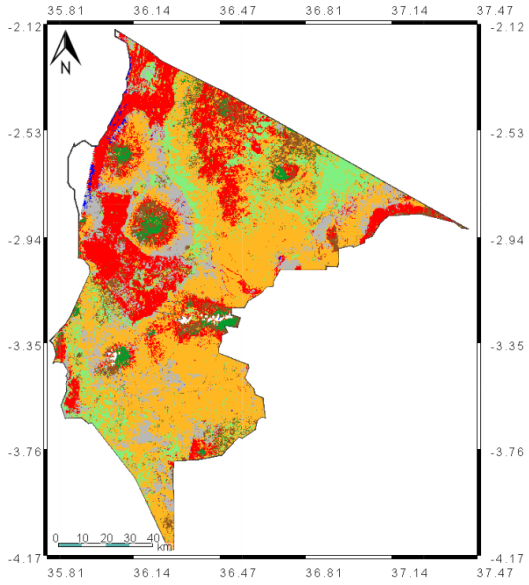

(b) 17 Oct 1988 (dry season)

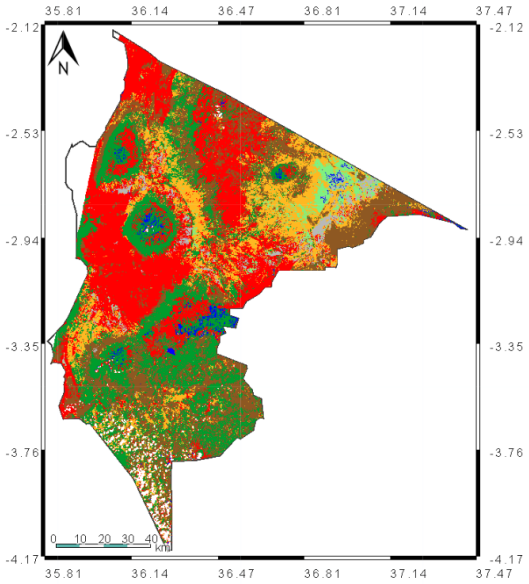

(c) 29 Jan 2018 (wet season)

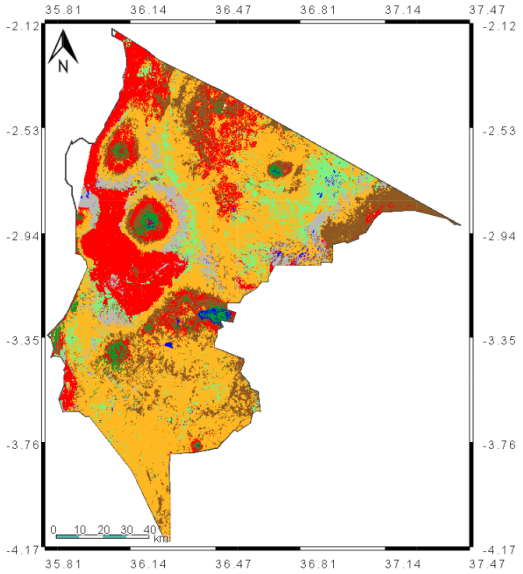

(d) 23 Sep 2017 (dry season)

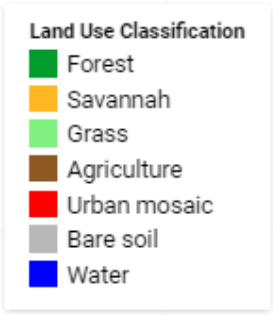

(e) Legend

Figure D.2: Land cover maps based on dataset 1,grouped classes.
Source: https://code.earthengine.google.com/e521ec70bd8e6d45ebf1382e32e7a9d6

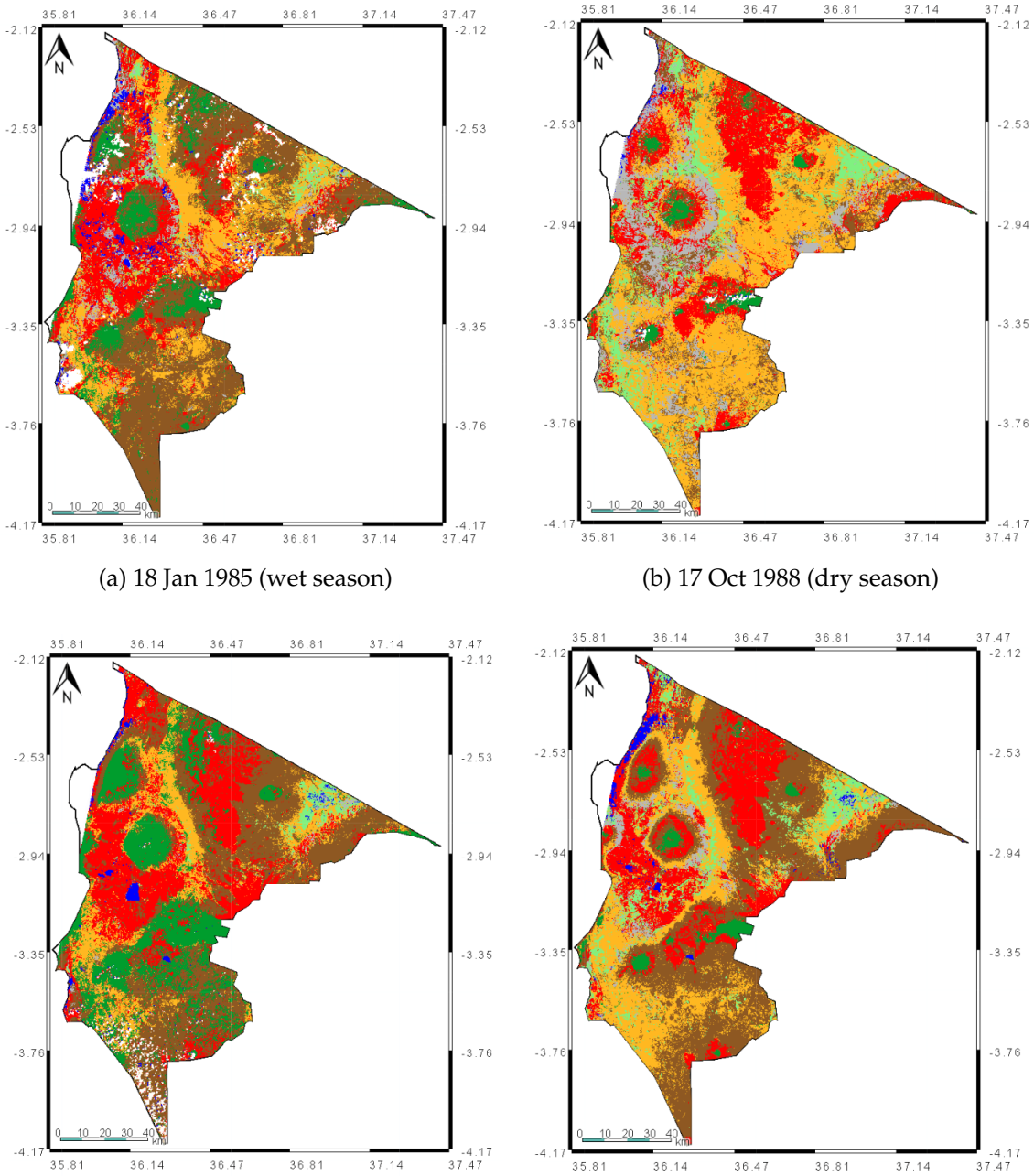

(a) 18 Jan 1985 (wet season)

(b) 17 Oct 1988 (dry season)

(c) 29 Jan 2018 (wet season)

(d) 23 Sep 2017 (dry season)

Figure D.3: Land cover maps based on dataset 2.
Source: https://code.earthengine.google.com/00b0795e2d0b3eb0c5ea454b9711b011

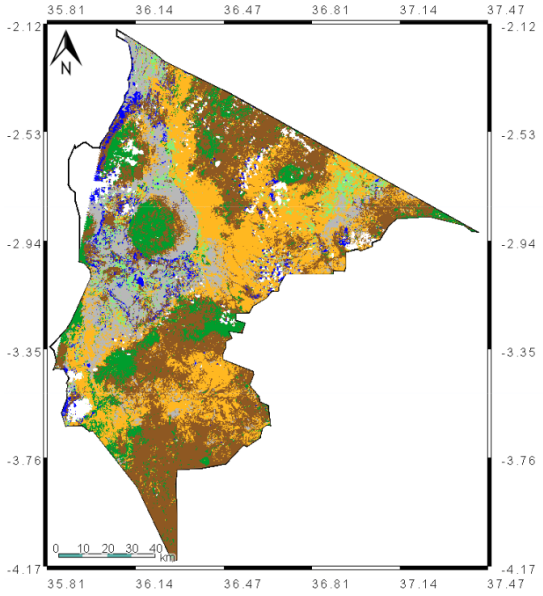

(a) 18 Jan 1985 (wet season)

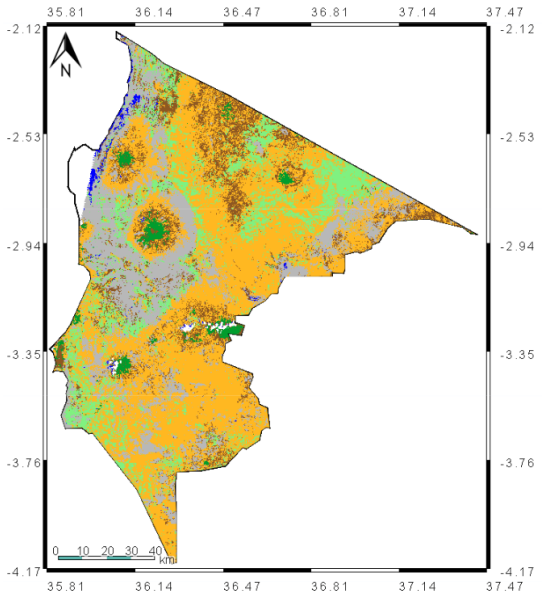

(b) 17 Oct 1988 (dry season)

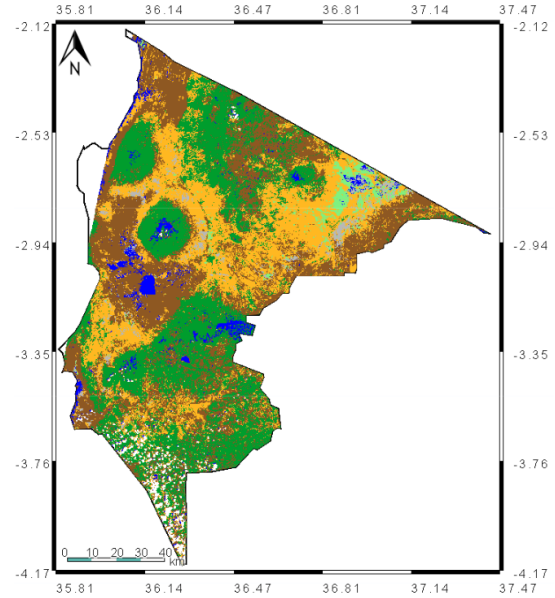

(c) 29 Jan 2018 (wet season)

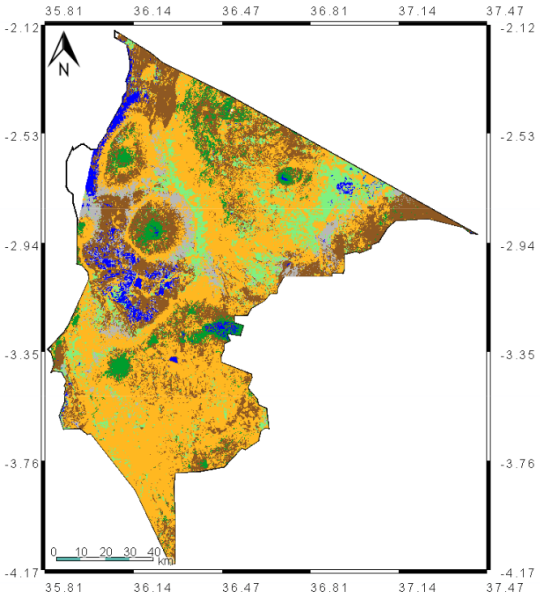

(d) 23 Sep 2017 (dry season)

Figure D.4: Land cover maps based on dataset 3.
Source: https://code.earthengine.google.com/32893721359e0d2eea39a5582e5f098f

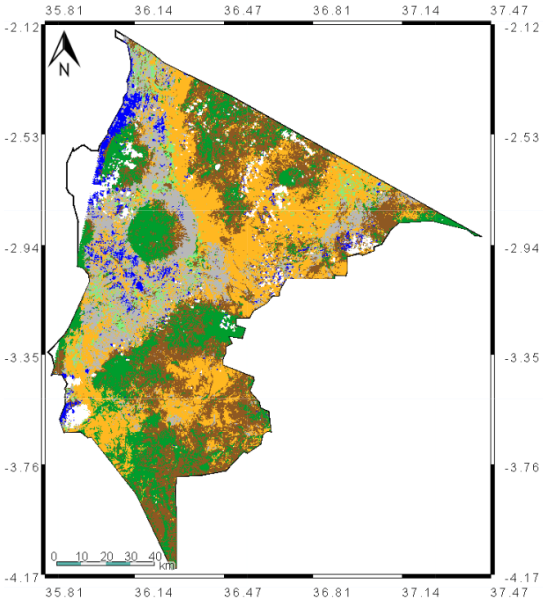

(a) 18 Jan 1985 (wet season)

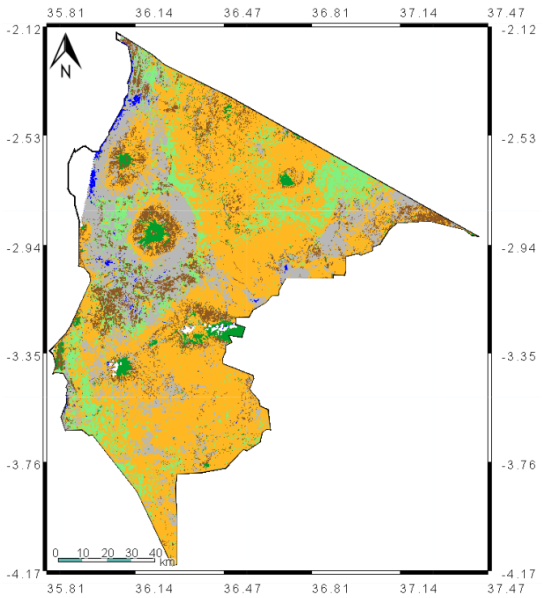

(b) 17 Oct 1988 (dry season)

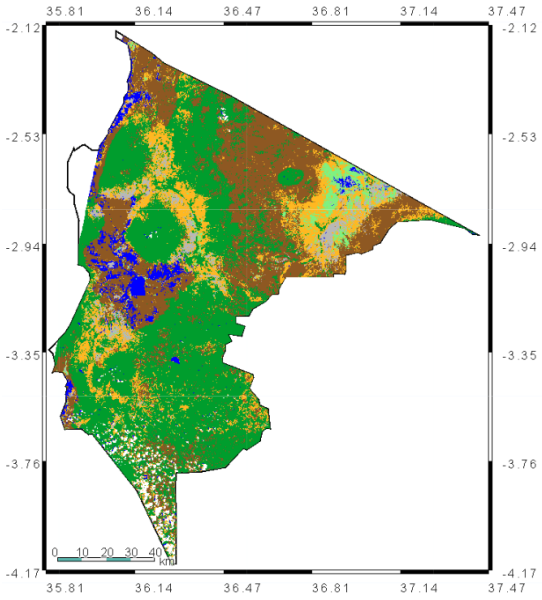

(c) 29 Jan 2018 (wet season)

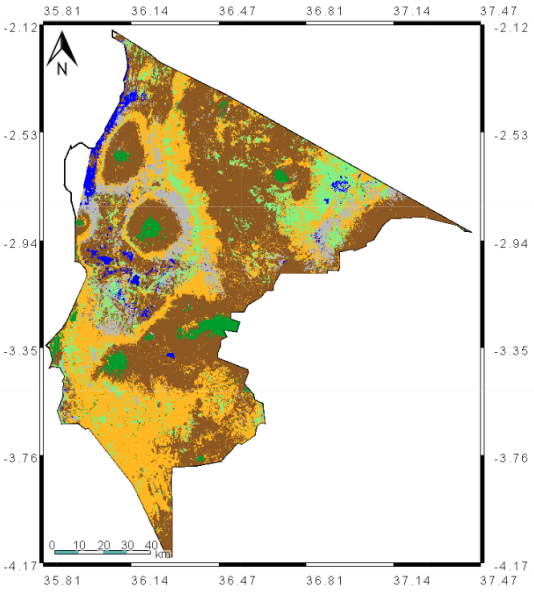

(d) 23 Sep 2017 (dry season)

Figure D.5: Land cover maps based on dataset 4.
Source: https://code.earthengine.google.com/1702c8ccea390f3c2952b3344d4d7587

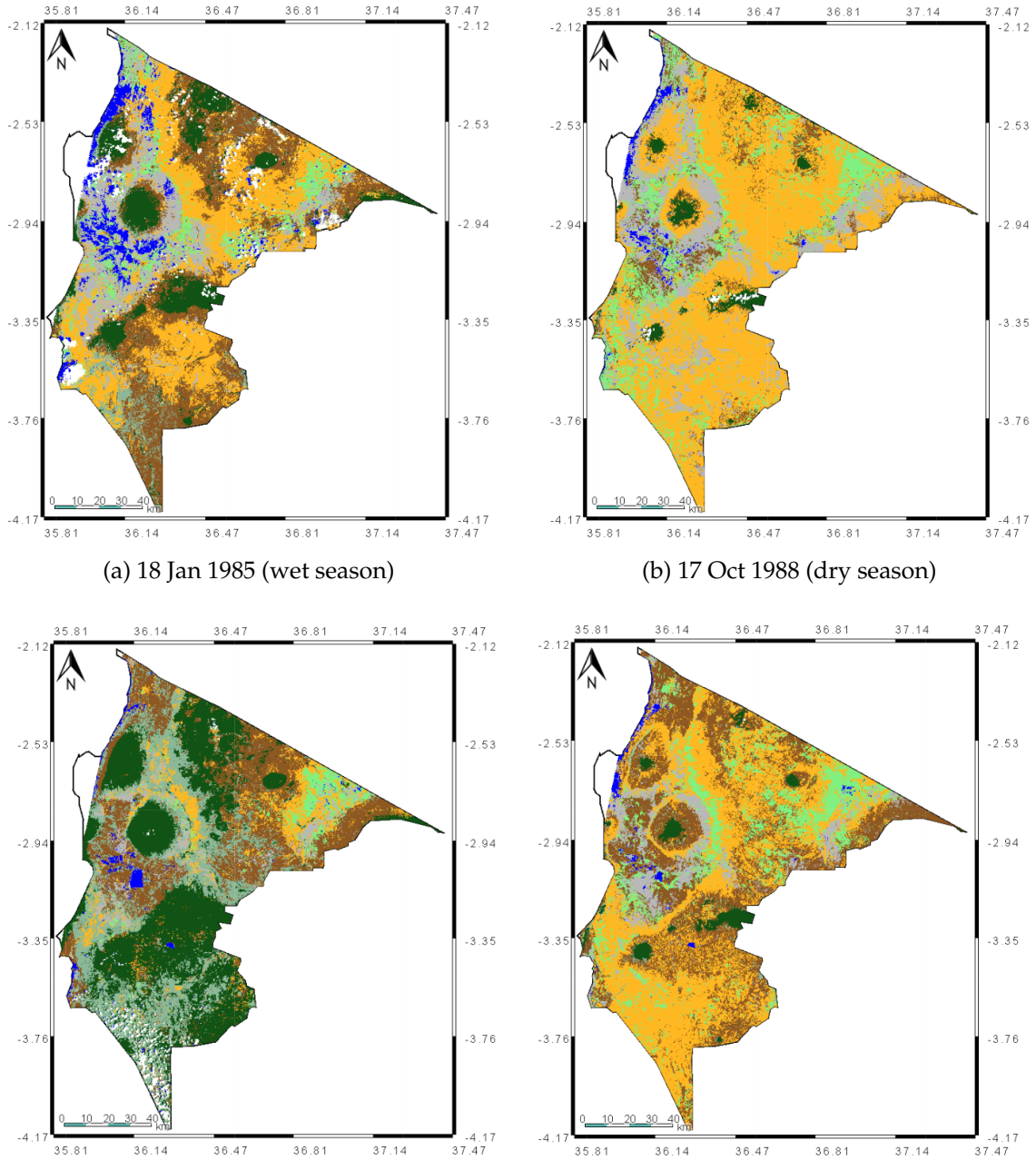

(a) 18 Jan 1985 (wet season)

(b) 17 Oct 1988 (dry season)

(c) 29 Jan 2018 (wet season)

(d) 23 Sep 2017 (dry season)

Figure D.6: Land cover maps based on dataset 5.
Source: https://code.earthengine.google.com/c79563f2c0b776a93d795bf1a4c93c23

Appendix E Vegetation dynamics, NDVI

Table E.1: Coordinates of the locations of teach NDVI trend analysis area.
Source: https://code.earthengine.google.com/83649686817bad89ed9609e5502bec43

Area	Lat	Lon
Grass (north)	36.863	-2.786
	36.854	-2.798
	36.872	-2.807
	36.882	-2.790
	36.906	-2.718
	36.900	-2.730
	36.913	-2.732
	36.916	-2.717
Ricefields	35.859	-3.375
	35.859	-3.375
	35.860	-3.375
	35.860	-3.375
	35.859	-3.375
	35.859	-3.375
	35.859	-3.375
	35.859	-3.375
Intercrop (maize, beans, sunflower)	35.864	-3.319
	35.865	-3.320
	35.865	-3.320
	35.866	-3.320
	35.866	-3.320
	35.866	-3.320
	35.865	-3.320
	35.865	-3.319
	35.872	-3.329
	35.871	-3.330
	35.874	-3.330
	35.873	-3.328
	35.860	-3.291
	35.864	-3.291
	35.864	-3.290
	35.866	-3.289
	35.867	-3.287
	35.861	-3.287
	35.859	-3.289
	35.858	-3.344
	35.857	-3.344
	35.857	-3.347
	35.860	-3.347
	35.859	-3.345
	35.859	-3.345

Area	Lat	Lon
Grass (south)	35.909	-3.349
	35.903	-3.357
	35.908	-3.361
	35.916	-3.353
	35.930	-3.382
	35.925	-3.395
	35.932	-3.398
	35.943	-3.385
Savannah (south)	35.983	-3.489
	35.981	-3.491
	35.984	-3.493
	35.987	-3.490
	35.986	-3.468
	35.982	-3.472
	35.986	-3.476
	35.988	-3.470
	36.127	-3.712
	36.123	-3.730
	36.147	-3.735
	36.152	-3.715
Forest	36.086	-3.376
	36.081	-3.378
	36.083	-3.382
	36.090	-3.380
	35.844	-3.372
	35.841	-3.376
	35.847	-3.377
	35.847	-3.373
	36.233	-2.880
	36.226	-2.885
	36.230	-2.894
	36.242	-2.887
	36.476	-3.257
	36.475	-3.261
	36.481	-3.261
	36.482	-3.257
	36.702	-2.697
	36.697	-2.703
	36.714	-2.707
	36.714	-2.697

Area	Lat	Lon
Savannah (north)	36.660	-2.562
	36.660	-2.574
	36.687	-2.573
	36.685	-2.560
	36.853	-2.687
	36.841	-2.706
	36.878	-2.709
	36.867	-2.687
	36.276	-2.503
	36.269	-2.552
	36.335	-2.540
Banana plantations	35.853	-3.356
	35.853	-3.358
	35.855	-3.357
	35.849	-3.353
	35.850	-3.354
	35.851	-3.353
	35.861	-3.371
	35.861	-3.373
	35.862	-3.373
	35.861	-3.371
	35.853	-3.371
	35.853	-3.371
	35.854	-3.369
	35.853	-3.369
	35.854	-3.366
	35.855	-3.367
	35.855	-3.367
	35.856	-3.366
	35.853	-3.355
	35.855	-3.354
	35.854	-3.353
	35.854	-3.354
	35.863	-3.354
	35.863	-3.354
	35.864	-3.354
	35.864	-3.354

Table E.2: The amount of images per location used for the NDVI time series analysis. Split into the total amount of images (Total), the amount of images before the year 2000 (<2000), the amount of images from Landsat 4 or 5 (TM), Landsat 7 (ETM), and Landsat 8 (OLI-TIRS).

Location	Grass N	Grass S	Forest	Sav. N	Sav. S	Rice	Banana	Intercrop
Total	362	761	713	387	756	435	673	697
<2000	23	44	38	26	63	25	34	42
TM	34	70	63	35	112	38	54	68
ETM	213	413	402	223	455	212	374	383
OLI-TIRS	115	278	248	129	189	185	245	246

Table E.3: The average NDVI and the coefficient of variation (CV) during the different seasons at each location (interannual).

		Grass N	Grass S	Forest	Sav. N	Sav. S	Rice	Banana	Intercrop
NDVI	Wet season	0.179	0.334	0.732	0.321	0.373	0.517	0.621	0.461
	Dry season	0.115	0.151	0.658	0.181	0.190	0.440	0.567	0.346
	Yearly	0.154	0.240	0.687	0.266	0.277	0.444	0.599	0.381
CV	Wet season	34.11	29.82	9.16	28.33	31.60	17.30	11.93	21.54
	Dry season	21.73	20.67	9.88	17.42	35.96	26.20	14.62	22.52
	Yearly	33.86	30.53	10.18	29.44	29.97	21.22 9	10.29	27.30

Table E.4: The correlation between long term monthly averaged NDVI and rainfall, calculated with Kendall's τ. The lag is the shift in months to obtain the highest significance and correlation. Other lags could also improve the fits.

	Grass N	Grass S	Forest	Sav. N	Sav. S	Rice	Banana	Intercrop
p-value	0.000	0.000	0.002	0.000	0.000	0.153	0.009	0.009
T	58	60	55	60	58	55	52	52
tau	0.758	0.818	0.667	0.818	0.758	0.333	0.576	0.576
lag	1	1	1	1	1	0	2	2

Appendix F Climate data trend tests

Table F.1: The Mann-Kendall trend test was applied on long term rainfall data. The data was obtained from three meteostations (Karatu, Babati and Monduli) and averaged if two datapoints were available and left out if only one datapoint was available. The monthly rainfall data was aggregated into seasonal data, divided into short dry (Jan-Feb), long rain (Mar-May), long dry (Jun-Oct), short rain (Nov-Dec) and the hydrological year (Aug-Jul).

Average 3 stations	Short dry	Long rain	Long dry	Short rain	Hydrological year
Score	132	-124	-65	61	-14
Var(score)	8513	5846	6327	6834	5390
Denominator	860.5	666	703	741	630.0
tau	0.153	-0.186	-0.0925	0.0823	-0.0222
2 sided p-value	0.156	0.108	0.421	0.468	0.859

Table F.2: The Mann-Kendall trend test was applied on long term rainfall data. The data was obtained from Karatu meteostation. The monthly rainfall data was aggregated into seasonal data, divided into short dry (Jan-Feb), long rain (Mar-May), long dry (Jun-Oct), short rain (Nov-Dec) and the hydrological year (Aug-Jul).

Karatu	Short dry	**Long rain**	Long dry	Short rain	Hydrological year
Score	49	**-177**	5	77	-1
Var(score)	7365.7	**6833.7**	5845	5845	4550.3
Denominator	779.5	**741**	665.5	665.5	561
tau	0.629	**-0.239**	0.00751	0.116	-0.00178
2 sided p-value	0.576	**0.033**	0.958	0.320	1

Table F.3: The Mann-Kendall trend test was applied on long term rainfall data. The data was obtained from Babati meteostation. The monthly rainfall data was aggregated into seasonal data, divided into short dry (Jan-Feb), long rain (Mar-May), long dry (Jun-Oct), short rain (Nov-Dec) and the hydrological year (Aug-Jul).

Babati	Short dry	Long rain	Long dry	Short rain	Hydrological year
Score	78	13	27	10	36
Var(score)	5846	4958.3	4531.7	4165.3	1625.3
Denominator	666	595	555.0	528	276
tau	0.117	0.0218	0.0487	0.0189	0.13
2 sided p-value	0.314	0.865	0.699	0.889	0.385

Table F.4: The Mann-Kendall trend test was applied on long term rainfall data. The data was obtained from Monduli meteostation. The monthly rainfall data was aggregated into seasonal data, divided into short dry (Jan-Feb), long rain (Mar-May), long dry (Jun-Oct), short rain (Nov-Dec) and the hydrological year (Aug-Jul).

Monduli	Short dry	Long rain	Long dry	Short rain	Hydrological year
Score	70	-30	-104	58	-44
Var(score)	8513.3	6326	7924.7	9129.3	5390
Denominator	860.5	702.5	819.0	902.5	630.0
tau	0.0813	-0.0427	-0.127	0.0643	-0.0698
2 sided p-value	0.455	0.715	0.247	0.551	0.558

Table F.5: The Mann-Kendall trend test was applied on long term temperature data. The data was obtained from Arusha Airport meteostation. The mean monthly minimum temperature and mean monthly maximum temperature were averaged to annual minimum and annual maximum.

	Min	Max
Score	420	184
Var(score)	6828	6326
Denominator	738.5	702.5
tau	0.569	0.262
2 sided p-value	0.000	0.021

Appendix G Sediment displacement in gully systems

Sheet wash and consequent soil erosion has been causing loss of topsoil and incision of flow convergence lines in many parts of the Monduli and Longido district. As stated by the research of Blake et al. (2018), local herders have noticed that gully erosion has become more severe over the last 15 years. Overgrazing has been found to be the main cause of sheet erosion development in the specific research area defined by Blake et al. (2018), although gully erosion was found both in overgrazed areas and along livestock routes. In a study by Hammond Murray-Rust (1972) a subbasin of 9.3 km^2 on the southern slope of the Monduli Mountain was analysed on the causes of soil erosion. Here the total sediment yield was 5.798 tons/(ha $\cdot$ y) during a 9 year period, which increased almost 1.5 times in the subsequent two years (Hammond Murray-Rust, 1972). The sediment is transported to downstream area's. Lake Manyara is an endorheic basin where (seasonal) rivers from the Monduli district flow towards to. Due to long periods of droughts and short but intensive rainfall events, significant amounts of soil are eroded and transported to Lake Manyara, which increases the risk of reservoir sedimentation. A major source of sediment is from gully erosion, although the occupied land is often $<$5% of the area of a catchment (Ionita et al., 2015).

In order to get an idea of the sediment displacement from gullies within the Lake Manyara watershed and the possible sediment deposition in the lake, two gully systems between Mto wa Mbu and Makuyuni were studied. From Google Earth data it is clear that gully systems in the area develop every rainy season (Figure G.1). To get an insight of the magnitude of total sediment loss at a gully or during a specific time period, two gullies were measured. In situ data was collected about the width, depth, typology (V/U shape) and length of the gully. This was done prior to the long rains, and repeated after two months.

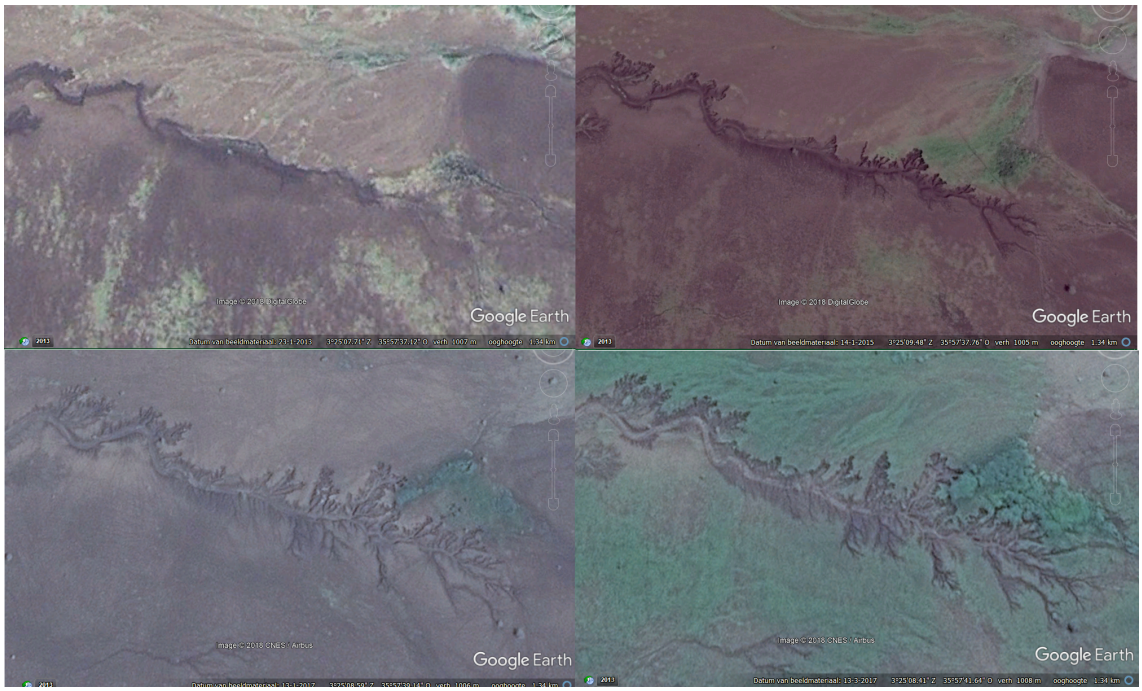

Figure G.1: Satellite imagery of a gully in Monduli district (3.41°S, 35.96°N) expanding through time: January 2013 (upperleft), January 2015 (upper right), January 2017 (lower left) and March 2017 (lower right). Source: Google Earth (2013)

The gully to be investigated was chosen based on accessibility, size and signs of (recent) growth. The width and depth of the gully were measured with respect to the un-

certainties described by Casalí et al. (2015). The gully width and depth were measured at every 5 meters in order to get a proper profile of the system. The depth was measured on an interval of 0.5 meters. A metal pole was put on both sides of the gully and a rope was tight in between, 10 cm above the soil at the pin. An interval of 0.5 m was marked on the rope, at which the depth was determined from that marking to the gully bottom. This procedure was repeated after two months at the same location. With the collected data a point cloud can be made, from which the loss of sediment can be calculated. This will give more information about the displacement of sediment in the gully system.

Two gullies were measured (Image G.2 and G.3). The data of these gullies has been added as supplementary data in a .csv file.

Figure G.2: Gully 1. Location: 3 29 18.9433S, 35 59 45.7137E

Figure G.3: Gully 2. Location: 3 27 32.84S, 35 58 17.0190E